Investigating the impacts of climate change on hydroclimatic extremes in the Tar-Pamlico River basin, North Carolina

Thanh-Nhan-Duc Tran[a, *], Mahesh R Tapas[b], Son K. Do[a], Randall Etheridge[c] and Venkataraman Lakshmi[a]

[a] Department of Civil and Environmental Engineering, University of Virginia, Charlottesville, VA 22904, USA

[b] Integrated Coastal Programs, East Carolina University, Greenville, NC 27858, USA

[c] Department of Engineering, Center for Sustainable Energy and Environmental Engineering, East Carolina University, Greenville, NC 27858, USA

*Corresponding author: syu3cs@virginia.edu (Thanh-Nhan-Duc Tran)

The 16-digit ORCID: 0000-0001-8478-5893 (Thanh-Nhan-Duc Tran)

Abstract

Evaluating the forthcoming impacts of climate change is important for formulating efficient and flexible approaches to water resource management. General Circulation Models (GCMs) are primary tools that enable scientists to study both past and potential future climate changes, as well as their impacts on policies and actions. In this work, we quantify the future projected impacts of hydroclimatic extremes on the coastal, risk-prone Tar-Pamlico River basin in North Carolina using GCMs from the Sixth International Coupled Model Intercomparison Project (CMIP6). These models incorporate projected future societal development scenarios (Shared Socioeconomic Pathways, SSPs) as defined in the Intergovernmental Panel on Climate Change (IPCC) Sixth Assessment Report (AR6). Specifically, we have utilized historical residential expansion data, the Soil and Water Assessment Tool Plus (SWAT+), the Standardized Precipitation Index (SPI), and the Interquartile Range (IQR) method for analyzing extremes from 2024 to 2100. Our findings include: (1) a trend toward wetter conditions is identified with an increase in flood events toward 2100; (2) projected increases in the severity of flood peaks are found, quantified by a rise of 21% compared to the 2000–2020 period; (3) downstream regions are forecast to experience severe droughts up to 2044; and (4) low-lying and coastal regions are found as particularly susceptible to higher flood peaks and more frequent drought events between 2045 and 2100. This work provides valuable insights into the anticipated shifts in natural disaster patterns and supports decision-makers and authorities in promoting adaptive strategies and sustainable policies to address challenges posed by future climate changes in the Tar-Pamlico region and throughout the state of North Carolina, United States.

Keywords: Climate change; Flood; Drought; CMIP6; Resilience; Tar-Pamlico River basin.

1. Introduction

Many countries, including the United States, have an extensive history of dealing with natural disasters (Easterling et al., 2000). Many works indicated that changes in the intensity and frequency of these extreme events could significantly impact human lives (Bonsoms et al., 2023; Guan et al., 2021; Kang et al., 2022; Saadi et al., 2024; Sanjay Mankar et al., 2020; Tran et al., 2022d, 2023b, 2023e; Donnelly et al., 2024a). Weather-related extreme events such as droughts and floods, which vary spatially and temporally, can considerably affect local communities (Anjanee Prabha and Tapas, 2020; Cao et al., 2023; Dias et al., 2024; IPCC, 2013; Omojola et al., 2012; Tan et al., 2023; Trenberth et al., 2014; Zhang et al., 2023; Zhou et al., 2023; Noori et al., 2023). Specifically, floods and droughts can lead to severe fatalities and cause significant losses in country's economy (Garner et al., 2017; Ma and Yuan, 2021; Ren et al., 2023; Thibeault and Seth, 2014; Tran et al., 2021a, 2021b; Zhang et al., 2024; Donnelly et al., 2024b). The frequency and severity of these events are projected to increase significantly with rising temperatures and greater precipitation intensities (Aryal et al., 2023; Mishra et al., 2023; Nguyen et al., 2023; Tran et al., 2022a). In the United States, Porter et al. (2021) indicated that the projected risk for human properties could increase up to 10% under climate change impacts. Additionally, Hsiao et al. (2021) and Masciopinto and Liso. (2016) found that these impacts are even more substantial in low-lying regions.

Human-related factors could further intensify extreme weather events (Hansen and Stone, 2016). The latest Intergovernmental Panel on Climate Change (IPCC) report highlights the expected rise in temperature and CO2 concentrations, primarily due to human activities (Carter et al., 1994; IPPC, 2021). An increase of at least 1.5 ◦C above pre-industrial levels in global temperatures is projected within the next two decades (Carter et al., 1994; Chen et al., 2020; Hansen and Stone, 2016; IPPC, 2021; Yun et al., 2021). A recent work by Raftery et al. (2017), using a statistically-based probabilistic approach, indicated there is only a 1% chance of preventing this phenomenon. In addition, this is expected to escalate the frequency and severity of floods and droughts, especially in coastal regions (IPCC, 2021, 2019). Global increases in greenhouse gas emissions from anthropogenic sources could intensify water-related issues (Hansen and Stone, 2016; IPCC, 2019; Nguyen et al., 2022; Rosenzweig and Neofotis, 2013; Song et al., 2022; Trang et al., 2017). Future hydroclimatic extremes would then result in severe impacts, such as sea-level rise (Mahdian et al., 2024), coastal flooding (Kang et al., 2022; Mafi-Gholami et al., 2020; Masciopinto and Liso, 2016), increased storm intensity (Hsiao et al., 2021), changes in salinity (Loc et al., 2021; Park et al., 2022), and economic losses (Lien, 2019). These impacts are particularly pronounced in agriculture (Parajuli et al., 2019) and coastal watersheds (IPPC, 2021; Mafi-Gholami et al., 2020). Besides, coastal regions face unique challenges compared to other areas, mainly due to their low altitude (Baills et al., 2020; Toimil et al., 2020), lack of natural-based measurements (O'Donoghue et al., 2021), and exacerbating factors such as urbanization (Gopalakrishnan et al., 2019).

The Tar-Pamlico River basin, which is the fourth-largest watershed in North Carolina, has been selected for future climatic investigations due to its unique geographical and socioeconomic characteristics (NC DEQ, 1994). This is also motivated by the region's significant agriculture activities that are increasingly threatened by climate change (Mulligan et al., 2019; Osmond et al., 2015). In addition, this region, where fifty-five percent of the land comprises forests and wetlands, is currently vulnerable to environmental risks such as seawater intrusion, sea-level rise, and land degradation that are likely to be exacerbated by future climate (NC DEQ, 1994). Tapas et al. (2022a) developed a hydrological model for the Tar-Pamlico basin, which incorporates stakeholders' inputs. Their preliminary results revealed that local farmers are increasingly threatened by climate change, a finding found by their discussions with the locals and authorities. Thus, given its high socioeconomic and ecological value, immediate action is necessary to protect the region's agriculture and human well-being from hydroclimatic extremes (Mulligan et al., 2019). Furthermore, despite escalating global climate change impacts this decade (Chen et al., 2020; Hansen and Stone, 2016; Mahdian et al., 2023), as of this writing, no studies have been published investigating the climate change impacts on this region. This research gap has thus become the primary motivation for our work, which aims to support authorities and stakeholders in developing sustainable plans to mitigate future climate impacts on this area.

General Circulation Models (GCMs) are important for quantifying impacts of future projected hydroclimatic extremes (Neill et al., 2016; Tebaldi et al., 2021). GCMs theoretically simulate the physics, chemistry, and biology of the atmosphere, land, and oceans in great detail (Tebaldi et al., 2021). The latest version of the Coupled Model Intercomparison Project Version V6 (CMIP6) was recently released with updates (Neill et al., 2016). Specifically, it introduces a new concept of the Scenario Model Intercomparison Project, which is based on the Shared Socioeconomic Pathways (SSPs) (Eyring et al., 2016). This marks a significant milestone of the IPCC's global project with the integration and consideration of socioeconomic factors (IPPC, 2021; Meyer, 2015), as highlighted in the IPCC AR6 report (IPPC, 2021). SSP outlines specific scenarios of greenhouse gas emissions (e.g., SSP2–45 and 5–85) and Land Use Land Cover (LULC) changes under baseline scenarios (Neill et al., 2016). Incorporating these emission scenarios into hydrological models enables a better understanding of the physical impacts of climate and societal factors on hydrological processes (Neill et al., 2016). Additionally, selecting appropriate CMIP6 GCMs is critical due to various factors such as resolution (Di Virgilio et al., 2022) and geographical characteristics of the region (Tebaldi et al., 2021). In this study, we use the NASA Earth Exchange Global Daily Downscaled Projections – NASA NEX-GDDP-CMIP6 (Thrasher et al., 2022), which has been utilized and validated in previous works (Chen et al., 2020; Dias et al., 2024; Park et al., 2023; Saadi et al., 2024). In this study, four GCMs have been selected for their proven efficiency in recent works: BCC-CSM2-MR from the Beijing Climate Center, China Meteorological Administration (China); CanESM5 from the Canadian Center for Climate Modeling and Analysis (Canada); MIROC6 from the Japan Agency for Marine-Earth Science and Technology and the Atmosphere and Ocean Research Institute at the University of Tokyo (Japan); and MRI-ESM2-0 from the Meteorological Research Institute (Japan) (Chen et al., 2022; Peng et al., 2023; Wang et al., 2021; Xu et al., 2023) (see Section 2.2).

In this study, our aim is to quantify the impacts of GCMs under SSP scenarios on future climatic extremes in the Tar-Pamlico River basin, North Carolina state. We employed the Standardized Precipitation Index (SPI), the semi-distributed hydrological Soil and Water Assessment Tool Plus (SWAT+) model, and the Interquartile Range (IQR) method for analysis across three timeframes: the near future (2024–2044), mid future (2045–2069), and far future (2070–2100). Our primary objectives are to understand and evaluate the impacts of climate change on hydroclimatic extremes, mainly focusing on S1-3 regions (see Section 2.1). We aim to first (a) reveal projected changes in future meteorological variables, then (b) quantify the intensity and frequency of future flood and drought events, and lastly (c) discuss the forecasted impacts of these extremes on these regions. Additionally, we provide a general analysis on the historical residential expansions (population and housing units) in the S1-3 regions from 1990 to 2020, using data from the U.S. Census Bureau, the North Carolina Department of Environmental Quality (NC DEQ), and the United States Geological Survey (USGS) Land Change Monitoring, Assessment, and Projection (LCMAP) data sets (USGS, 2020) (Fig. 1). The materials and methods will be presented in Section 2, results in Section 3, discussions of the findings in Section 4, limitations and potential future work in Section 5, and the conclusions in Section 6.

2. Materials and methods

2.1. Study area

The Tar-Pamlico River basin has been selected for this study due to its distinctive hydrological modeling characteristics because of its significance to the North Carolina state, United States (Fig. 1). This basin drains into the Pamlico Sound, supporting a unique and diverse ecosystem of habitats (Keith, 2014; NC DEQ, 1994, 2009). It covers an area of approximately 14,428 km^2 (about 5,571 mi^2), extends across 15 counties, and supports a total population of over 470,000 (Keith, 2014; NC DEQ, 2009).

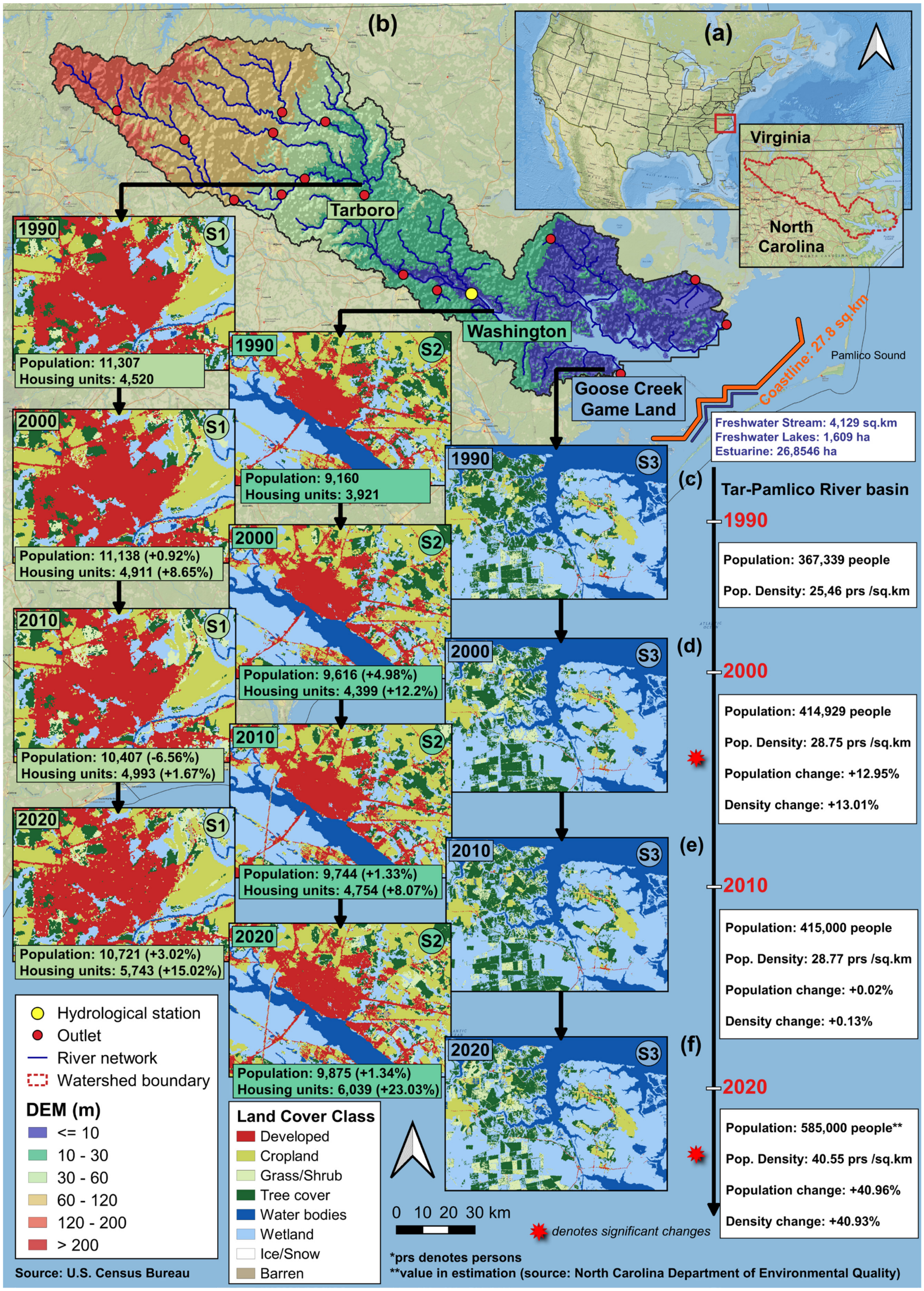

Fig. 1. (a) Location of the Tar-Pamlico River basin within the United States; (b) Terrain profiles and geographical characteristics of the Tar-Pamlico watershed; (c–f) LULC changes and historical residential

expansions, including population and housing units, in the (S1) Tarboro, (S2) Washington, and (S3) Goose Creek Game Land regions, using LCMAP data sets (1990–2020) (USGS, 2020) with the colors encoded to corresponding regions (S1–S3). The region's historical residential expansions, including population growth, housing units, and their densities are calculated based on data from the U.S. Census Bureau (U.S. Census Bureau, 2022; Center for Sustainable Systems, 2023) and NC DEQ (NC DEQ, 2020). The percentage change (%) indicates the difference between the latter year and the previous year.

The Tar-Pamlico River basin features a diverse distribution of land use, with forests covering 33.9%, wetlands 31.9%, and agricultural land 27.9% of the area (NC DEQ, 2009). The freshwater streams and rivers within the basin have their origins in the agriculturally rich, wetland-dense, and forested areas of the Piedmont region in north-central North Carolina. These waterways flow southeastward and, upon nearing tidal zones, transform into expansive, tidally influenced estuaries (Keith, 2014). These estuaries eventually feed into the Tar-Pamlico Sound (Fig. 1b), enhancing its ecological complexity and economic productivity (NC DEQ, 1994, 2009). The basin's distinct terrain profiles, LULC distribution, and climatic characteristics make it an ideal area for this study. In this study, we mainly focus on three regions, including (S1) the town of Tarboro and (S2) the city of Washington, which have been selected due to their socioeconomic importance (Fig. 1), as well as (S3) the Goose Creek Game Land region, chosen because of its vulnerability to seawater intrusion and ecological significance (NC DEQ, 1994, 2009) (Fig. 1).

2.2. Descriptions of GCMs and SSP scenarios

We used the NASA NEX-GDDP-CMIP6 dataset, which was downscaled and bias-corrected with a spatial resolution of approximately 25 × 25 km (Thrasher et al., 2022). This dataset covers two "Tier 1" SSP scenarios, namely SSPs 2-45 and 5-85 (Neill et al., 2016; Thrasher et al., 2022). These CMIP6 GCMs were designed to support the objectives of the IPCC AR6, focusing on capturing climate projections based on various socioeconomic scenarios (IPPC, 2021). The datasets have been downscaled using the Bias-Correction Spatial Disaggregation method with the aim to address common constraints in GCM outputs (Maurer and Hidalgo, 2008; Wood et al., 2002, 2004). The efficiency of GCMs is affected by different factors, such as the model's algorithm and baseline conditions, resulting in divergent precision levels in simulating particular basins and regions (Chen et al., 2020). Studies by Park et al. (2023) and Thrasher et al. (2022) highlighted that the BCC-CSM2-MR, CanESM5, MIROC6, and MRI-ESM2-0 models show good applications in future climate investigations, and thus they have been chosen in this study. Besides, Chen et al. (2022) and Xu et al. (2023) indicated the good performance of these GCMs in capturing a wide range of future streamflow changes, while Wang et al. (2021) indicated that CanESM5 and BCC-CSM2-MR show unique advantages in producing satisfactory results in terms of precipitation.

Specifically, these models show good correlations compared to the other GCMs (Wang et al., 2021). Besides, Peng et al. (2023) highlighted that MIROC6 and MRI-ESM2-0 have the highest reliabilities in temperature and precipitation, outperforming the other 17 GCMs. Our analysis was conducted on two SSP scenarios, as the intermediate (SSP2-45) and high-end (SSP5-85) greenhouse gas emission levels (Thrasher et al., 2022). The summary of the these GCM models is presented in Table 1.

Table 1.

Description of the chosen GCMs used in this study.

No	Model	Country	Description
1	BCC-CSM2-MR	China	Beijing Climate Center China Meteorological Administration
2	CanESM5	Canada	Canadian Centre for Climate Modelling and Analysis, Environment and Climate Change Canada, Canada
3	MIROC6	Japan	Japan Agency for Marine-Earth Science and Technology (JAMSTEC), Japan & Atmosphere and Ocean Research Institute (AORI), The University of Tokyo, Japan & National Institute for Environmental Studies, Japan (NIES) & RIKEN Center for Computational Science, Japan (R-CCS)
4	MRI-ESM2-0	Japan	Meteorological Research Institute, Japan

2.3. Hydrological SWAT+ model

SWAT model was developed by the United States Department of Agriculture Agricultural Research Service (USDA-ARS) in the mid-1990s and is one of the most advanced, open-source models for a wide range of hydrological applications (Tran et al., 2022b, 2023a). SWAT is primarily utilized for simulating hydrological processes within various water management regimes (Tran et al., 2023d). In this study, we used the SWAT+ version, a restructured update of SWAT, released in 2017. While retaining the core hydrological and computational algorithms of the original model, SWAT+ introduces additional features to better represent spatial distributions. These enhancements are centered around the rainfall-runoff concept and the water balance equation (Arnold et al., 2012; Gassman et al., 2007; Tran & Lakshmi, 2022).

Many studies have used this model to investigate the impacts of various factors on streamflow and sediment loads. These factors include changes in land cover (Ahmed et al., 2020; Cheng et al., 2018), climate change impacts (Aslam et al., 2022; Shafeeque et al., 2023a, 2023b), sustainability of ecosystem services (Ashrafi et al., 2022a, 2022b; Behboudian et al., 2021; Umar et al., 2022), applications of satellite-based products (Arshad et al., 2021, 2022; Aryal et al., 2023; Noor et al., 2023; Tran et al., 2022c, 2023c; Tapas et al., 2023), and groundwater contamination by agricultural chemicals (Trang et al., 2017).

2.3.1. Model setup and workflow

The boundary of the Tar-Pamlico River basin, which is used in the SWAT+ model, was extracted from the USGS StreamStats (Ries et al., 2017). Figure 2 shows the schematic workflow of our study, highlighting the main stages along with the model's inputs and outputs. We utilized SWAT+ (version 3.16.9) and the Quantum Geographic Information System (QGIS) software for SWAT+ (Dile et al., 2019) for the model run in this study (Dile et al., 2019) (Fig. 2). Additionally, the Terrain Analysis Using Digital Elevation Models (TauDEM) version 5.0 was used within SWAT+ model for watershed delineation (Tarboton, 2011).

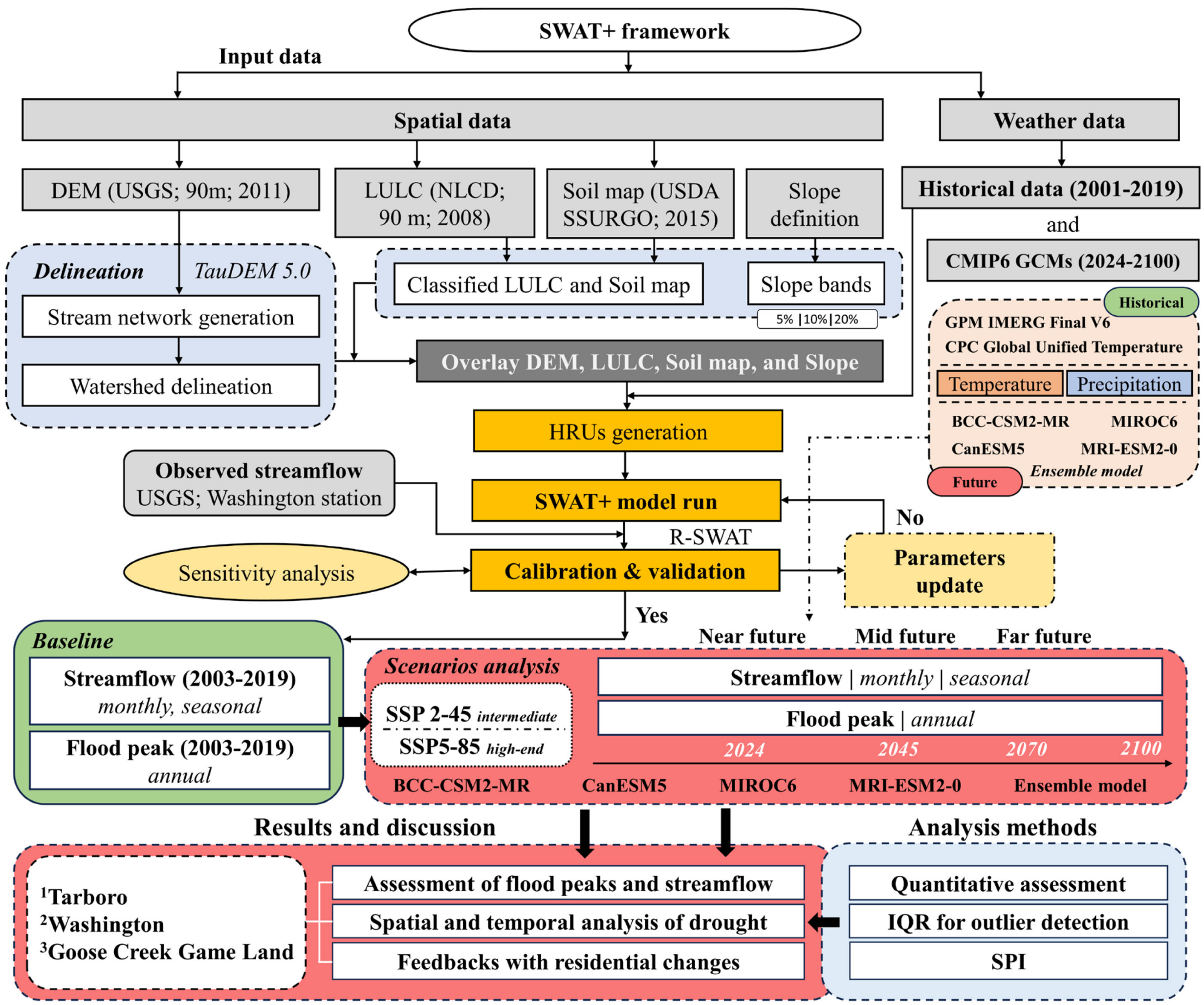

Fig. 2. The schematic flowchart used in this study. First, we prepared the needed data sets, which include historical data and projected data sets from CMIP6 GCMs (see Section 2.2). Calibration and validation were conducted at the Washington hydrological station (Fig. 1b). The calibrated model values were then used to simulate SSP scenarios from 2024 to 2100. Assessments were carried out over the Tar-Pamlico

River basin and at three selected sites: Tarboro, Washington, and Goose Creek Game Land (Fig. 1b). Additional analyses incorporated residential expansion data and LULC changes.

For the SWAT+ model, we conducted watershed extraction and analyzed hydrologic information derived from the DEM input. This analysis was essential to delineate streams, sub-basins, and create Hydrological Response Units (HRUs) (Arnold et al., 2012; Pignotti et al., 2017). Specifically, the watershed was divided into smaller sub-watersheds that contain distinctive characteristics from the DEM, LULC, and soil characteristics that were stored in HRUs. An HRU in SWAT+ represents the smallest spatial unit (Arnold et al., 2012), where the water balance equation is used for calculations in each pixel within the watershed, ensuring that hydrological processes are accounted for from the upstream to the downstream region (Figs. 1 and 2) (Douglas-Mankin et al., 2010; Neitsch et al., 2011; Gassman et al., 2007).

The DEM data for the year 2011, with a 90 m resolution, was obtained from the USGS website (USGS, 2020) (Fig. 2). LULC data were collected from the USGS National Land Cover Database (NLCD), based on a survey in 2008 (Yang et al., 2018). In addition, the soil data were acquired from the USDA Soil Survey Geographic Database (SSURGO) for the year 2015 (USDA, 2010).

To calibrate and validate the SWAT+ model, we utilized data from the USGS database for the Washington hydrological station (Figs. 1b and 2), covering the period from 2001 to 2019. It is important to note that this observation includes gaps, primarily due to tidal influence, which can result in negative flow values. Thus, before using this data in the model calibration, we converted these negative flow values to zeros, as the SWAT+ model is unable to process backflow (Bieger et al., 2017). This specific adjustment ensures that negative flows are treated as low flows, considering the limitations of one-dimensional flow modeling (Arnold et al., 2012; Bieger et al., 2017).

In this study, we have chosen the initial two years (2001 and 2002) for the warm-up period for the SWAT+ model. The calibration period was chosen between 2003 and 2011 while the validation period was chosen (2012-2019) (Fig. 2). We performed a total of 5,000 iterations for each scenario at a monthly scale. Besides, future climate scenarios were simulated using inputs from the selected GCM SSPs and an ensemble model combining all GCMs (2024-2100). These simulations used the calibrated parameters extracted from the historical scenario (2003-2019) (Fig. 2). Our analysis was divided into three different future periods: the near future (2024-2044), the mid future (2045-2069), and the far future (2070-2100).

2.3.2. R-SWAT for model calibration and validation

We used the interactive web-based application R-SWAT for model calibration and validation. This application is developed using the R programming language and features open-source parallel processing capabilities (Nguyen et al., 2022).

Table 2.

Summary of the chosen parameters with their descriptions, change types, ranges, and units used for calibrating the SWAT+ model. This data are extracted from the SWAT+ documentation (SWAT+, 2018, 2020) with adjustments based on the Tar-Pamlico River basin's characteristics. Rank is the sensitivity ranking of parameters from the model's calibration and validation.

Rank	Name	Method	Min	Max	Description (unit)
1	cn2.hru	relative	– 0.30	0.20	SCS curve number for soil moisture condition 2 (null)
2	revap_co.aqu	absolute	– 0.10	0.10	Groundwater revap coefficient (null)
3	flo_min.aqu	relative	– 0.25	0.50	The lower limit of aquifer storage which enables return flow (m)
4	awc.sol	absolute	– 0.10	0.30	Available water capacity of the soil layer (mm_H2O/mm)
5	alpha.aqu	replace	0.01	0.50	Baseflow recession factor (days)
6	perco.hru	absolute	– 0.30	0.30	Percolation coefficient (fraction)
7	chk.rte	relative	– 0.25	0.25	Channel base conductivity (mm/hr)
8	cn3_swf.hru	absolute	– 0.30	0.50	The coefficient for pothole evaporation (null)
9	epco.hru	absolute	0	0.30	Plant uptake compensation factor (null)
10	esco.hru	absolute	0	0.30	Soil evaporation compensation factor (null)
11	k.sol	relative	– 0.25	0.25	Hydraulic conductivity (mm/hr)
12	ovn.hru	absolute	0	5	SCS curve number for soil moisture condition 2 (null)
13	surlag.bsn	replace	0.05	15	The coefficient for surface runoff lag (days)
14	evlai.bsn	replace	0	10	Leaf area index at zero evaporation from water bodies (null)
15	biomix.hru	absolute	– 0.30	0.30	Biological mixing efficiency (m)
16	nperco.bsn	absolute	0	1	Nitrate percolation coefficient (null)
17	lat_len.hru	relative	– 0.30	0.30	Slope length for lateral subsurface flow (m)

18	lat_orgn.aqu	relative	– 0.30	0.30	Organic N in the base flow (mg/L)
19	crk.bsn	absolute	0	1	Crack flow code (null)
20	field_len.fld	relative	– 0.30	0.30	Field length for wind erosion (m)
21	field_wid.fld	relative	– 0.30	0.30	Field width for wind erosion (m)
22	n_updis.bsn	absolute	0	30	Nitrogen uptake distribution parameter (null)
23	erorgp.hru	relative	– 0.30	0.30	Phosphorus enrichment ratio for loading with sediment (null)
24	dis_stream	relative	– 0.50	0.50	Average distance to stream (m)

For the calibration and validation of the SWAT+ model, we selected a total of 24 parameters using the R-SWAT application and employed the Generalized Likelihood Uncertainty Estimation (GLUE) calibration technique (Blasone et al., 2008) (Table 2). GLUE is a widely used algorithm in environmental system modeling due to its robustness (Tolson and Shoemaker, 2007). This technique involves randomly selecting numerous parameter combinations, with each set being assigned a likelihood score. This score reflects the probability of its occurrence across multiple model sets, based on how well the simulated values agree with the observed values, grounded in the principle of uniformity (Blasone et al., 2008; Mirzaei et al., 2015). In the SWAT+ model, the calibration (.cal) file delineates the absolute minimum and maximum ranges for these parameters. For parameters pertaining to aquifer levels, we used the "*replace*" method. This approach was chosen because SWAT+ typically assigns uniform values to all aquifers within a watershed, which can result in a loss of resolution at the aquifer level (Blasone et al., 2008; Tolson and Shoemaker, 2007; Mirzaei et al., 2015).

2.4. Performance metrics

In our study, the model's outputs are evaluated using the Kling-Gupta efficiency (KGE) (Gupta et al., 2009), Nash-Sutcliffe efficiency (NSE) (Nash and Sutcliffe, 1970), and Coefficient of determination (R^2) (Moriasi et al., 2015) (Table 3). The NSE assesses the proportion of the variance in the observed data that is quantified by the model (Nash and Sutcliffe, 1970). The KGE offers a thorough assessment by taking into account the comparisons of averages and variability, as well as the correlation between observed and simulated streamflow (Gupta et al., 2009; Saeedi et al., 2022). R^2 measures the degree to which fluctuations in the observed factor are accounted for by the simulated variable (Moriasi et al., 2015). The ranges and equations of these metrics are shown in Table 3.

Table 3.

Summary of the model performance metrics used in this study.

Metric	Equation	Range
NSE	$1-\frac{\sum_{i=1}^{n}(Q_{obs}-Q_{sim})^2}{\sum_{i=1}^{n}(Q_{obs}-\overline{Q_{obs}})^2}$	VG: NSE ≥ 0.8; G: 0.7 ≤ NSE < 0.8; S: 0.5 ≤ NSE < 0.7; NS: NSE < 0.5
KGE	$1-\sqrt{(CC-1)^2+\left(\frac{{Q_{sim}}^{d}}{{Q_{obs}}^{d}}-1\right)^2+\left(\frac{\overline{Q_{sim}}}{\overline{Q_{obs}}}-1\right)^2}$	VG: KGE ≥ 1; G: 0.50 ≤ KGE ≤ 1; S: 0 ≤ KGE ≤ 0.50; NS: KGE < 0
R^2	$\frac{\left[\sum_i\left(Q_{obs,i}-\overline{Q_{obs}}\right)\left(Q_{sim,i}-\overline{Q_{sim}}\right)\right]^2}{\sum_i\left(Q_{obs,i}-\overline{Q_{obs}}\right)^2\sum_i\left(Q_{sim,i}-\overline{Q_{sim}}\right)^2}$	VG: R^2 ≥ 0.8; G: 0.7 ≤ R^2 < 0.8; S: 0.5 ≤ R^2 < 0.7; NS: R^2 < 0.5

Note: Q_{obs} is observed streamflow, Q_{sim} is simulated streamflow, i is i^{th} simulation, and $\bar{Q}$ is the mean value, and n is the total number of values. Very Good (VG), Good (G), Satisfactory (S), and Not Satisfactory (NS).

2.5. IQR method for Anomaly Detection of Future Flood Peaks

IQR is a statistical tool used for identifying outliers within a dataset (Wan et al., 2014). It divides the dataset into three quartiles, providing an overview of data distribution.

- 1st quartile represents the 25th percentile, also known as the median of the dataset's lower half (Q1).
- 2nd quartile represents the 50th percentile or the overall median of the dataset (Q2).
- 3rd quartile represents the 75th percentile, also known as the median of the dataset's upper half (Q3).

We first obtained the SWAT+ simulated flood peak on a monthly scale and use as input for this method. By using the IQR method, we identified anomalies in future flood peaks (2024–2100), in which our analysis was segmented into three pre-defined periods. We established the IQR range as (Q3 – Q1) with the lower and upper bounds defined as lower bound equals to [Q1 – (1.5 × IQR)] and upper bound equals to [Q3 + (1.5 × IQR)]. Peak values found outside these bounds are considered anomalies. By performing the IQR method over different periods, we highlight years with remarkably high and low peaks, indicating potential risks. This systematic approach enhances our understanding of potential flood risks in future scenarios.

2.6. Evaluation of projected drought events

It is crucial to establish criteria for quantifying the intensity and frequency of extreme events (Liu et al., 2021; Tapas et al., 2022b; Zhong et al., 2022). In this work, we used SPI for our analysis, with different levels of severity categorized using the US Drought Monitor (Svoboda et al., 2002) (Table 4). To be specific, dry conditions are identified when the SPI values fall below zero and keep decreasing to less than negative one (− 1). In contrast, a drought event is considered to have ended when these values return to positive, in which wet conditions are identified when the SPI values reach to positive two (+2) and beyond (Liu et al., 2021; Zhong et al., 2022).

We defined two evaluation indices: Severity (S) and Intensity (IDe). First, S is measured as the absolute sum of all SPI values during the event, with the event duration defined as the number of months from the onset of the event to its conclusion, excluding the final month when the SPI returns to positive (Eq. (1)). IDe is calculated as the average SPI value over the drought duration (Eq. (2)). IDe serves as an indicator of the event's severity, where higher values indicate more severe conditions.

$$S = \left|\sum_{i=1}^{a} Index_i\right| \qquad (Eq.\ 1)$$

$$ID_e = \frac{S_i}{a} \qquad (Eq.\ 2)$$

where a is the duration of the event (months), ID_e is the intensity, and S_i represents the SPI value during the i-month of the event. The frequency (F) is calculated as the average number of events during a specified time range.

Table 4.

Summary of drought category and their ranges for SPI.

Drought category	SPI range
Extreme wet	Index ≥ + 2.0
Severe wet	+ 1.5 ≤ Index < + 2.0
Moderate wet	+ 1.0 ≤ Index < + 1.5
Near normal/mild wet	0 ≤ Index < + 1.0
Near normal/mild drought	– 1.0 ≤ Index < 0
Moderate drought	– 1.5 ≤ Index < – 1.0
Severe drought	– 2.0 ≤ Index < – 1.5
Extreme drought	Index ≤ – 2.0

3. Results

3.1. Overview of historical residential expansion

We found that the Tar-Pamlico River basin experienced an increase in population and housing units from 1990 to 2020 (Fig. 1). Specifically, there was a notable 40% increase in population growth and density in 2020 compared to 2010 (Fig. 1f). At the regional level, the S1-3 areas exhibited similar trends in population, but showed varying changes in housing units. Indeed, Tarboro (S1) and Washington (S2) experienced considerable urban expansion, particularly noticeable in the rise in housing units from 2010 to 2020 (Fig. 1). Despite a modest population growth in these regions (a maximum increase of 3% compared to 1990), the number of new housing units built increased steadily, peaking at a 23.03% increase by 2020. Conversely, the Goose Creek Game Land region (S3) maintained a relatively stable land use distribution (Fig. 1), preserving its largely natural state.

3.2. SWAT+ calibration and validation

We performed the sensitivity analysis parameters using a *p*-value threshold of 0.05. This means if a parameter has a *p*-value less than 0.05, then it is considered sensitive. Four parameters were identified as sensitive in this study, including cn2, revap_co, flo_min, awc, alpha, and perco (Table 2). Specifically, the baseflow (alpha parameter) and percolation coefficient (perco parameter) are sensitive in this basin. This indicates a significant ratio of infiltration, where surface water percolates into deeper soil layers, a result that is consistent with the storage routing technique described in Mapes and Pricope (2020).

The model calibration and validation for the period from 2003 to 2019 yielded good results. The model achieved an overall NSE of 0.71, KGE of 0.82, and R^2 of 0.78. During the calibration period (2003-2011), the model achieved an NSE of 0.72, a KGE of 0.84, and a R^2 of 0.76, while during the validation period (2012-2019), these values were 0.68, 0.77, and 0.81, respectively. These results are categorized as *"Good"* (see Table 3), particularly when considering the complex hydrodynamic influences in the area, e.g., dam and reservoir, and backwater effects in this coastal region (Keith, 2014). The results give confidence to the model's effectiveness and reliability in simulating and evaluating the impacts of climate change in the following sections.

3.3. Projected changes in temperature and precipitation

First, we examined changes in the average monthly temperature and precipitation across GCMs and SSPs (Table 5). The average monthly historical precipitation is found at approximately 85.58 mm, and rises to 87.56 mm under the SSP2-45 and 90.07 mm under the SSP5-85 using the ensemble model.

Table 5.

Projected changes in average monthly precipitation and temperature for the future period (2024-2100) compared to historical period (2003-2019). Increase (I) represents upward trends, while decrease (D) represents downward trends. Darker color denotes a higher increase. Ensemble is the combined model of four GCMs used in this study (see Table 1).

GCM	Temperature (ºC)				
	Maximum		Minimum		Trend
	SSP2-45	SSP5-85	SSP2-45	SSP5-85	
Ensemble	+ 3.77	+ 4.66	+ 0.86	+ 1.80	I
BCC-CSM2-MR	+ 3.72	+ 4.70	+ 0.49	+ 1.36	I
CanESM5	+ 4.14	+ 5.26	+ 1.44	+ 2.70	I
MIROC6	+ 3.66	+ 4.44	+ 0.64	+ 1.36	I
MRI-ESM2-0	+ 3.57	+ 4.25	+ 0.87	+ 1.77	I

	Precipitation (mm)		
	SSP2-45	SSP5-85	Trend
Ensemble	+ 1.98	+ 4.49	I
BCC-CSM2-MR	+ 1.60	+ 4.42	I
CanESM5	+ 1.64	+ 4.37	I
MIROC6	+ 0.49	+ 3.81	I
MRI-ESM2-0	+ 4.20	+ 5.37	I

MRI-ESM2-0, CanESM5, and BCC-CSM2-MR, under the SSP2-45 scenario, project increases in monthly precipitation of 4.20 mm, 1.64 mm, and 1.60 mm, respectively. Under the SSP5-85 scenario, these models consistently indicate even greater increases, with projected rises of 5.37 mm, 4.37 mm, and 4.42 mm, respectively (Table 5). These trends, consistent across all SSP scenarios, suggest a general rise in monthly precipitation, potentially leading to significant changes in future hydroclimatic patterns, including more frequent flooding events.

On the other hand, we noted that the average historical maximum and minimum temperatures are around 21.47°C and 10.97°C, respectively. However, these figures are projected to increase by at least 3.77°C for the maximum and 1.80°C for the minimum temperatures, observed using the ensemble model (Table 5). Under the SSP5-85, the projected minimum temperature increase could be as high as 4.66°C. Moreover, we found that individual GCMs suggest even higher temperature increases than the ensemble model. For instance, under the SSP2-45 scenario, the CanESM5 model forecasts the most significant increase in maximum temperature at +5.26°C, closely followed by the BCC-CSM2-MR model with a projected increase of 4.70°C. These projections emphasize the substantial and increasing risks associated with extreme heat, highlighting the need for careful observation in mitigating these climatic changes.

3.4. Projected changes in streamflow and flood peaks

Flood peak is an important outcome from numerical models that is essential for hydrological assessment (Merz et al., 2022). Figure 3 shows the projected flood peaks in the (a) Tarboro, (b) Washington, and (c)

Goose Creek Game Land regions for the near future (2024-2044), mid future (2045-2069), and far future (2070-2100) .

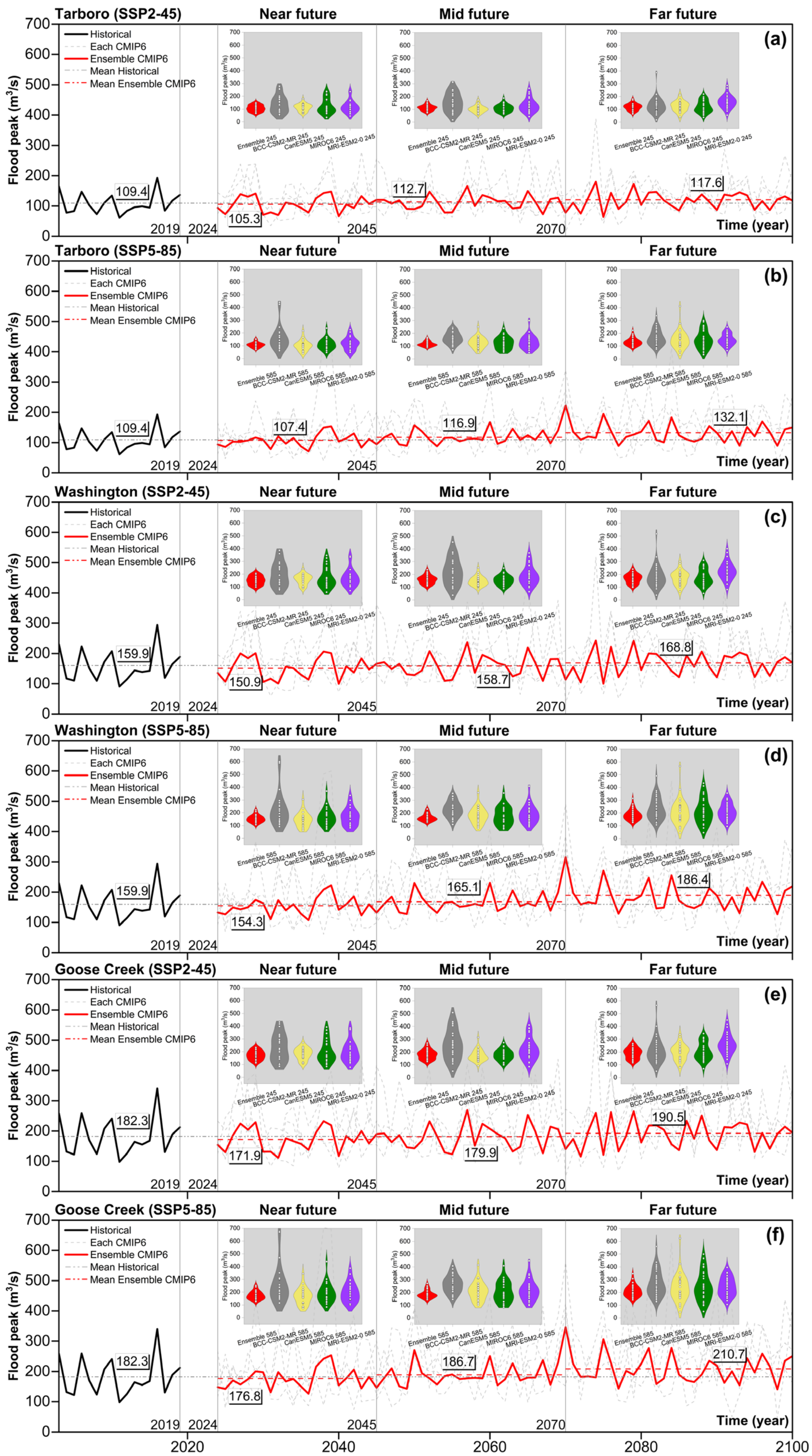

Fig. 3. Historical and projected flood peaks at (a-b) Tarboro, (c-d) Washington, and (e-f) Goose Creek Game Land. Future projections are simulated using the SWAT+ model, incorporating inputs from GCMs under different SSP scenarios (2-45 and 5-85). Black lines represent historical flood peaks (2003-2019), red lines represent the ensemble model (2024-2100), which combines the outputs from all GCMs, while dash grey lines show the projections from individual GCMs. Values in boxes represent mean flood peaks over different future periods (near, mid, and far) while the violin plots show the distribution of flood peaks from the ensemble models and individual GCMs.

In general, we found that higher flood peaks are likely to appear starting from 2045 across different examined regions (Fig. 3). While projected flood peaks in the near future (2024-2044) remain relatively unchanged compared to the historical period, the highest number of record-breaking peaks are frequently found in the far future (2070-2100), with the more severe greenhouse gas emission pathway (SSP5-85) showing higher peaks compared to SSP2-45. Specifically, when comparing historical flood peaks with future projected flood peaks, we observed that these increases range from 3 to 7% during the mid future and up to 21% during the far future. Moreover, when comparing Tarboro (S1) and Washington (S2), Tarboro—the more populated and higher housing density region (Fig. 1b)—shows a greater increase in flood peaks compared to Washington. To be specific, between mid- and far-future periods, mean flood peaks in Tarboro are expected to increase by 7.5% compared 5.5% in Washington under SSP2-45; and by 21% compared to 16.5% under SSP5-85, respectively. This could be explained by the higher impervious surface coverage in developed areas, which prevents water from infiltrating into the ground, exacerbating runoff and flooding issues. In addition, this could be exacerbated if the housing density continues to increase under the current growing population trend over the Tar-Pamlico River basin (see Section 3.1).

We also found that there are specific years within the near future (2024-2044) that are likely to experience notably high flood peaks. All of these regions are projected with significant flood peaks across various GCMs and SSPs between 2027 and 2039, as well as in 2042, indicating an elevated risk of flooding in this region (Figs. 3c, 3d, 3e, and 3f). Besides, the mean flood peak for this period is estimated to be approximately 179.9 m^3/s (under the SSP2-45 scenario) and 186.7 m^3/s (SSP5-85 scenario), respectively (Figs. 3e and 3f).

During the mid future (2044-2069), we observed notable trends and differences among GCMs and SSP scenarios. We found that the flood peak values oscillate between the upper bounds, formed by the MRI-ESM2-0 and MIROC6 models (significant years marked in 2052, 2057, 2060, 2065, and 2069), and the lower bounds delineated by the CanESM5 model (Fig. 3). There was a particularly noticeable increasing trend of flood peaks in the SSP5-85 scenarios, suggesting a trend towards wetter conditions. In Tarboro, our results show moderate fluctuations in flood peaks, with notable figures found under the SSP2-45 scenario, especially in the years 2052 and 2057 (Fig. 3a). Besides, Washington is projected to experience a higher volume and variability in future flood peaks, particularly during the 2060s, as compared to Tarboro due to its geographical location over the Tar-Pamlico River basin (Fig. 1b). In addition, Goose Creek Game Land region consistently exhibits the highest average flood peaks across all models in our analysis (Figs. 3e and 3f). This trend underscores the vulnerability of this low-lying, coastal region to climatic events that was previously highlighted by the NC Wildlife Resources Commission (NC Wildlife, 2018). Additionally, the ecological importance of the region and its susceptibility to potential flood risks underscore the need for strategic and adaptive planning to mitigate the impacts of these events. This includes, but is not limited to, strengthening flood defenses, enhancing ecological conservation efforts, and preparing comprehensive disaster response strategies.

For the far future (2070-2100) in Tarboro, our results indicate moderate fluctuations in flood peaks. Under the SSP2-45 scenario, a peak in 2074 (179.875 m^3/s) and a low in 2075 (64.025 m^3/s) are observed, while the SSP5-85 scenario projects a high peak at the beginning of the 2070s (notably in 2070 at 222.5 m^3/s), followed by lower projected flood peaks with moderate variability. In contrast, both the Washington and Goose Creek Game Land regions exhibit an increasing trend in projected flood peaks. In Washington, the highest peaks are projected in 2091 (242.75 m^3/s) and 2079 (221.75 m^3/s) under SSP2-45, while the SSP5-85 scenario projects even higher peaks, with 2070 (315.25 m^3/s) and 2075 (271.25 m^3/s) seeing the most significant increases. Similarly, the Goose Creek Game Land region demonstrates greater vulnerability compared to Tarboro and Washington. Its highest projected peak occurs in 2070 (346.5 m^3/s) under SSP5-85 and in 2079 (265.25 m^3/s) under SSP2-45. Additionally, across these regions between 2070 and 2100, there is an observed increase of 11.5% in flood peaks (SSP5-85) compared to the SSP2-45 scenario. This increase is more pronounced than the 3% increase observed during the mid-future period (2044-2069) and approximately 2% for the near future (2024-2044). This trend suggests that higher greenhouse gas emissions, as represented by the SSP5-85 scenario, tend to result in higher projected flood peaks, indicating a wetter trend toward the year 2100.

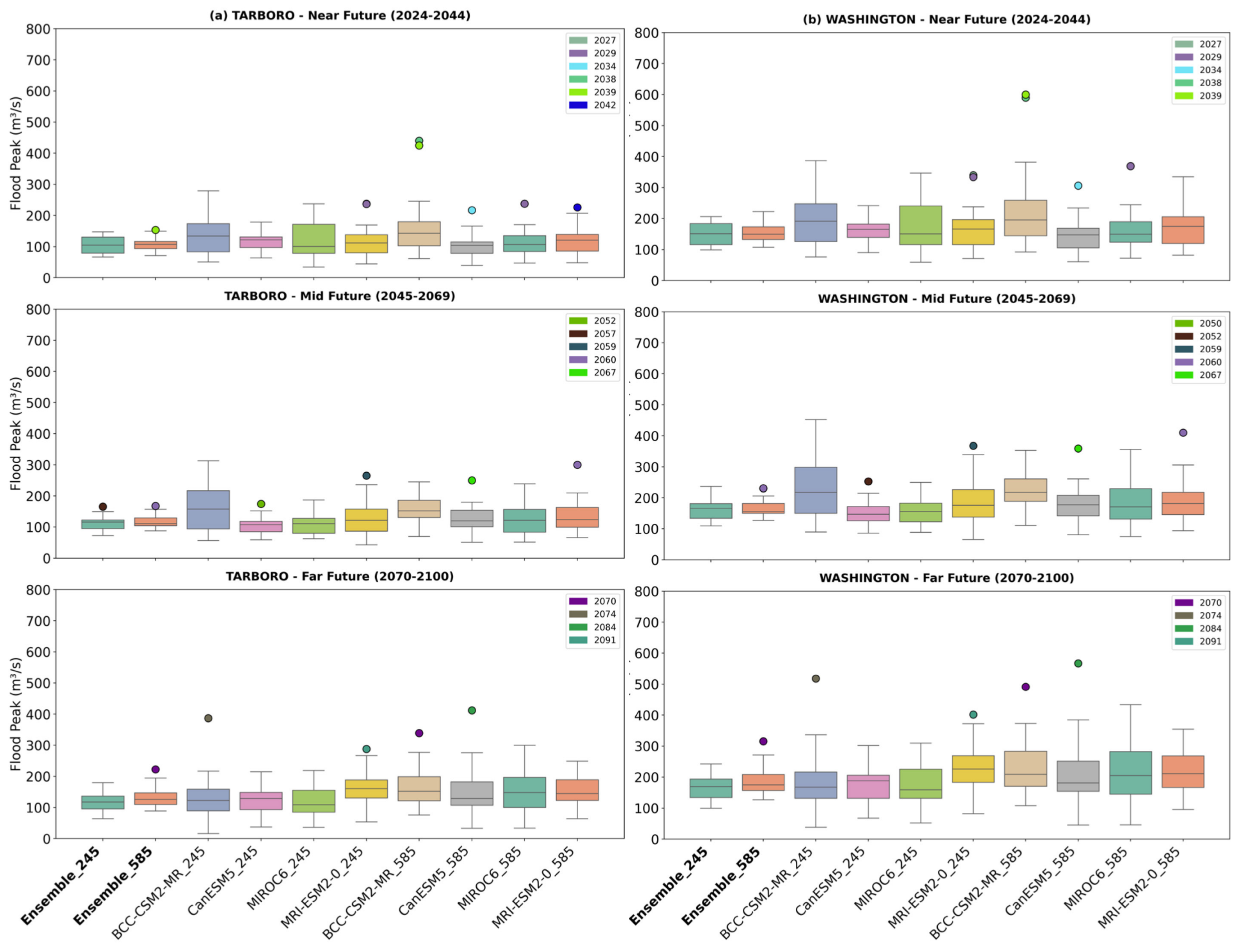
(a) TARBORO - Near Future (2024-2044)
(b) WASHINGTON - Near Future (2024-2044)
TARBORO - Mid Future (2045-2069)
WASHINGTON - Mid Future (2045-2069)
TARBORO - Far Future (2070-2100)
WASHINGTON - Far Future (2070-2100)
Flood Peak (m³/s)
2027
2029
2034
2038
2039
2042
2050
2052
2057
2059
2060
2067
2070
2074
2084
2091
Ensemble_245
Ensemble_585
BCC-CSM2-MR_245
CanESM5_245
MIROC6_245
MRI-ESM2-0_245
BCC-CSM2-MR_585
CanESM5_585
MIROC6_585
MRI-ESM2-0_585

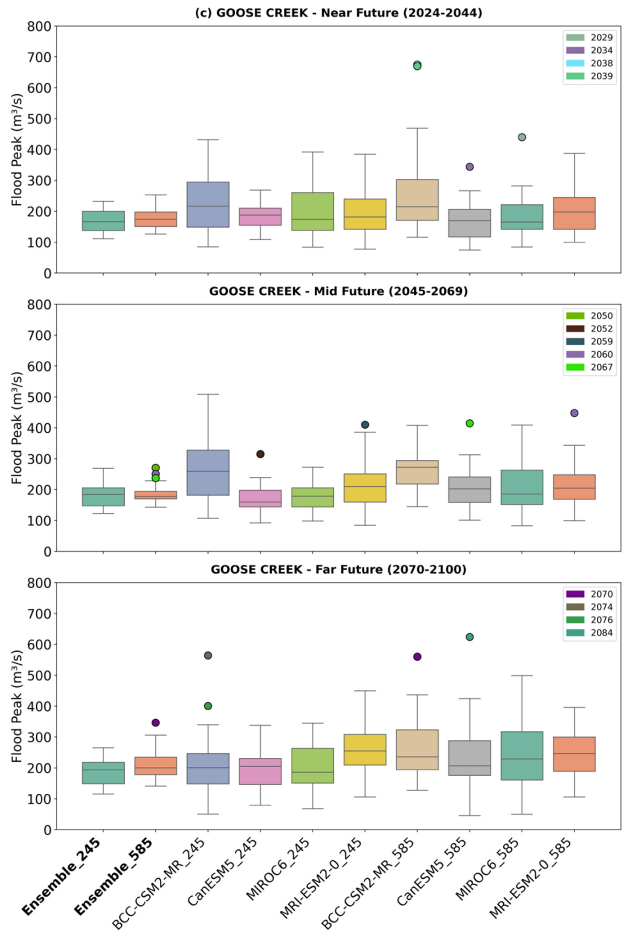

Fig. 4. Temporal anomalies of flood peaks using IQR method for (a) Tarboro, (b) Washington, and (c) Goose Creek Game Land station using the ensemble model and GCMs under the SSP2-45 and 5-85 scenarios, utilizing the IQR method. These analyses are conducted for different future periods, including the near future (2024-2044), mid future (2045-2069), and far future (2070-2100).

Extremely high or low flood peaks can significantly impact hydrological processes (Maurer et al., 2018), ecosystems (Yin et al., 2009), and human lives (Villarini and Smith, 2010). Thus, we utilized the IQR method (see Section 2.5) to identify variations in flood peaks from different GCMs under various SSPs. Figure 4 presents our findings on anomaly flood peaks over the three future periods - the near future (2024-2044), mid future (2045-2069), and far future (2070-2100) - for the (a) Tarboro, (b) Washington, and (c) Goose Creek Game Land regions. In general, we found an increase in flooding events from the near to the mid future across these regions (Fig. 4). The mid future period, in particular, shows a modest upward shift in median flood peaks across models, with notable outliers indicating the potential for occasional extreme flood events. In the far future, there is a considerable increase in both the variability and median values of flood peaks, especially under the MRI-ESM2-0 model (SSP5-85), indicating a trend towards more severe flooding. Across all three regions and various future periods, the MIROC6 and MRI-ESM2-0 models (SSP2-45 and 5-85) consistently show high medians and ranges for projected flood peaks, suggesting a correlation with more extreme weather events. Besides, as we move toward the far future (2070-2100), a clear trend of intensifying flood peaks is found (Fig. 4), highlighting the escalating impacts of climate change on these regions. We found that Tarboro is particularly susceptible to flooding, especially in 2029 and 2039 during the near future, with at least two GCMs predicting anomalies in the same years. The years 2060 and 2070 are identified as vulnerable for flooding in the mid and far future, respectively. In Washington, this is projected in 2029 (near future), 2060 (mid future), and 2070 (far future) while Goose Creek Game Land is in 2060 and 2067 (mid future), and 2070 (far future).

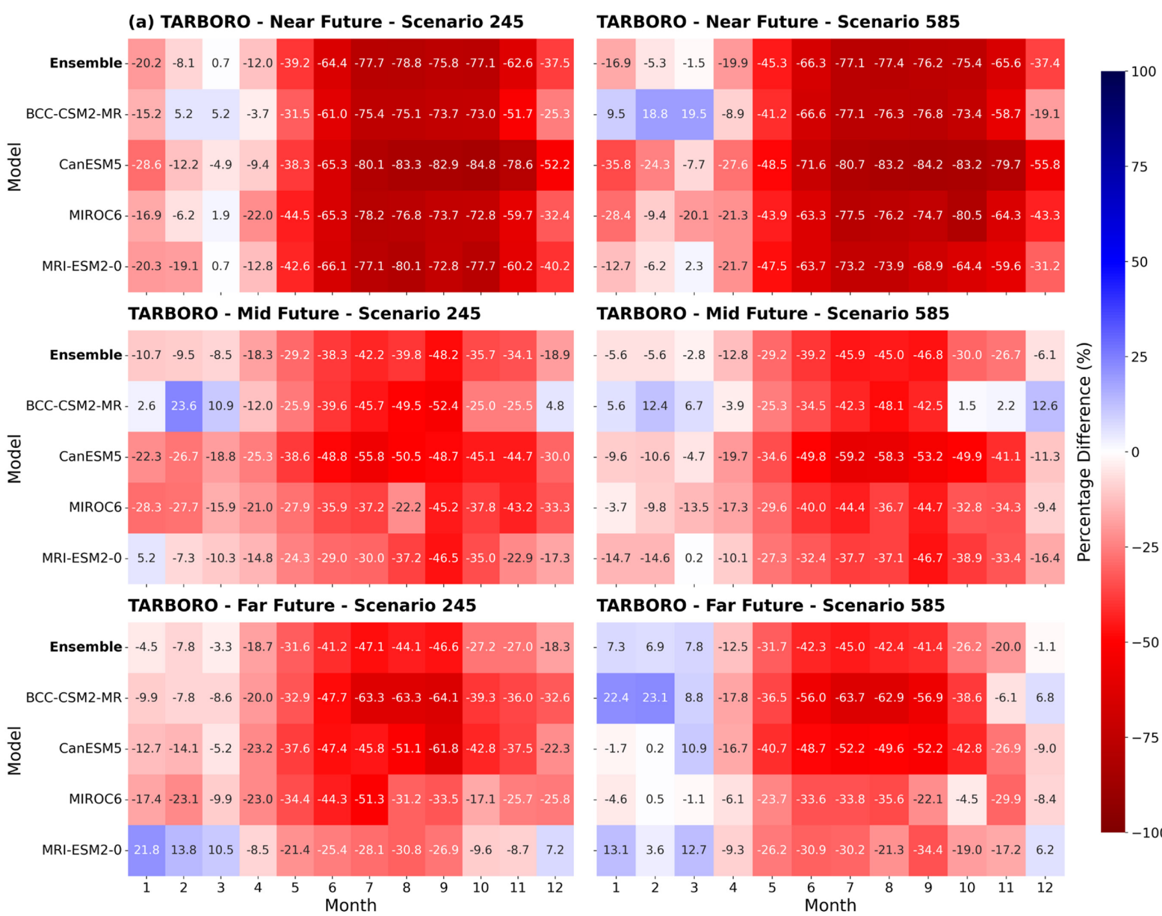

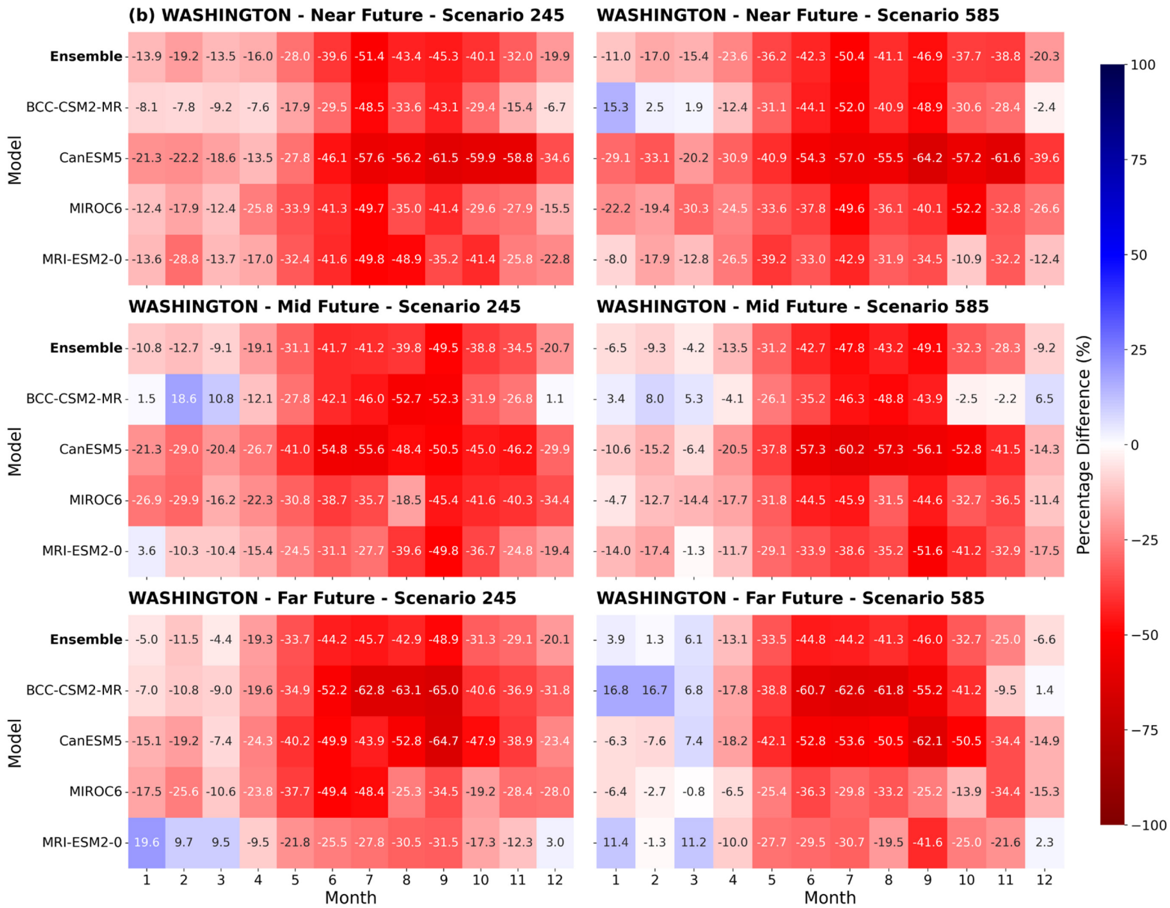
(b) WASHINGTON - Near Future - Scenario 245
WASHINGTON - Near Future - Scenario 585
WASHINGTON - Mid Future - Scenario 245
WASHINGTON - Mid Future - Scenario 585
WASHINGTON - Far Future - Scenario 245
WASHINGTON - Far Future - Scenario 585
Model
Ensemble
BCC-CSM2-MR
CanESM5
MIROC6
MRI-ESM2-0
Month
1 2 3 4 5 6 7 8 9 10 11 12
Percentage Difference (%)
100 75 50 25 0 −25 −50 −75 −100
-13.9 -19.2 -13.5 -16.0 -28.0 -39.6 -51.4 -43.4 -45.3 -40.1 -32.0 -19.9
-8.1 -7.8 -9.2 -7.6 -17.9 -29.5 -48.5 -33.6 -43.1 -29.4 -15.4 -6.7
-21.3 -22.2 -18.6 -13.5 -27.8 -46.1 -57.6 -56.2 -61.5 -59.9 -58.8 -34.6
-12.4 -17.9 -12.4 -25.8 -33.9 -41.3 -49.7 -35.0 -41.4 -29.6 -27.9 -15.5
-13.6 -28.8 -13.7 -17.0 -32.4 -41.6 -49.8 -48.9 -35.2 -41.4 -25.8 -22.8
-11.0 -17.0 -15.4 -23.6 -36.2 -42.3 -50.4 -41.1 -46.9 -37.7 -38.8 -20.3
15.3 2.5 1.9 -12.4 -31.1 -44.1 -52.0 -40.9 -48.9 -30.6 -28.4 -2.4
-29.1 -33.1 -20.2 -30.9 -40.9 -54.3 -57.0 -55.5 -64.2 -57.2 -61.6 -39.6
-22.2 -19.4 -30.3 -24.5 -33.6 -37.8 -49.6 -36.1 -40.1 -52.2 -32.8 -26.6
-8.0 -17.9 -12.8 -26.5 -39.2 -33.0 -42.9 -31.9 -34.5 -10.9 -32.2 -12.4
-10.8 -12.7 -9.1 -19.1 -31.1 -41.7 -41.2 -39.8 -49.5 -38.8 -34.5 -20.7
1.5 18.6 10.8 -12.1 -27.8 -42.1 -46.0 -52.7 -52.3 -31.9 -26.8 1.1
-21.3 -29.0 -20.4 -26.7 -41.0 -54.8 -55.6 -48.4 -50.5 -45.0 -46.2 -29.9
-26.9 -29.9 -16.2 -22.3 -30.8 -38.7 -35.7 -18.5 -45.4 -41.6 -40.3 -34.4
3.6 -10.3 -10.4 -15.4 -24.5 -31.1 -27.7 -39.6 -49.8 -36.7 -24.8 -19.4
-6.5 -9.3 -4.2 -13.5 -31.2 -42.7 -47.8 -43.2 -49.1 -32.3 -28.3 -9.2
3.4 8.0 5.3 -4.1 -26.1 -35.2 -46.3 -48.8 -43.9 -2.5 -2.2 6.5
-10.6 -15.2 -6.4 -20.5 -37.8 -57.3 -60.2 -57.3 -56.1 -52.8 -41.5 -14.3
-4.7 -12.7 -14.4 -17.7 -31.8 -44.5 -45.9 -31.5 -44.6 -32.7 -36.5 -11.4
-14.0 -17.4 -1.3 -11.7 -29.1 -33.9 -38.6 -35.2 -51.6 -41.2 -32.9 -17.5
-5.0 -11.5 -4.4 -19.3 -33.7 -44.2 -45.7 -42.9 -48.9 -31.3 -29.1 -20.1
-7.0 -10.8 -9.0 -19.6 -34.9 -52.2 -62.8 -63.1 -65.0 -40.6 -36.9 -31.8
-15.1 -19.2 -7.4 -24.3 -40.2 -49.9 -43.9 -52.8 -64.7 -47.9 -38.9 -23.4
-17.5 -25.6 -10.6 -23.8 -37.7 -49.4 -48.4 -25.3 -34.5 -19.2 -28.4 -28.0
19.6 9.7 9.5 -9.5 -21.8 -25.5 -27.8 -30.5 -31.5 -17.3 -12.3 3.0
3.9 1.3 6.1 -13.1 -33.5 -44.8 -44.2 -41.3 -46.0 -32.7 -25.0 -6.6
16.8 16.7 6.8 -17.8 -38.8 -60.7 -62.6 -61.8 -55.2 -41.2 -9.5 1.4
-6.3 -7.6 7.4 -18.2 -42.1 -52.8 -53.6 -50.5 -62.1 -50.5 -34.4 -14.9
-6.4 -2.7 -0.8 -6.5 -25.4 -36.3 -29.8 -33.2 -25.2 -13.9 -34.4 -15.3
11.4 -1.3 11.2 -10.0 -27.7 -29.5 -30.7 -19.5 -41.6 -25.0 -21.6 2.3

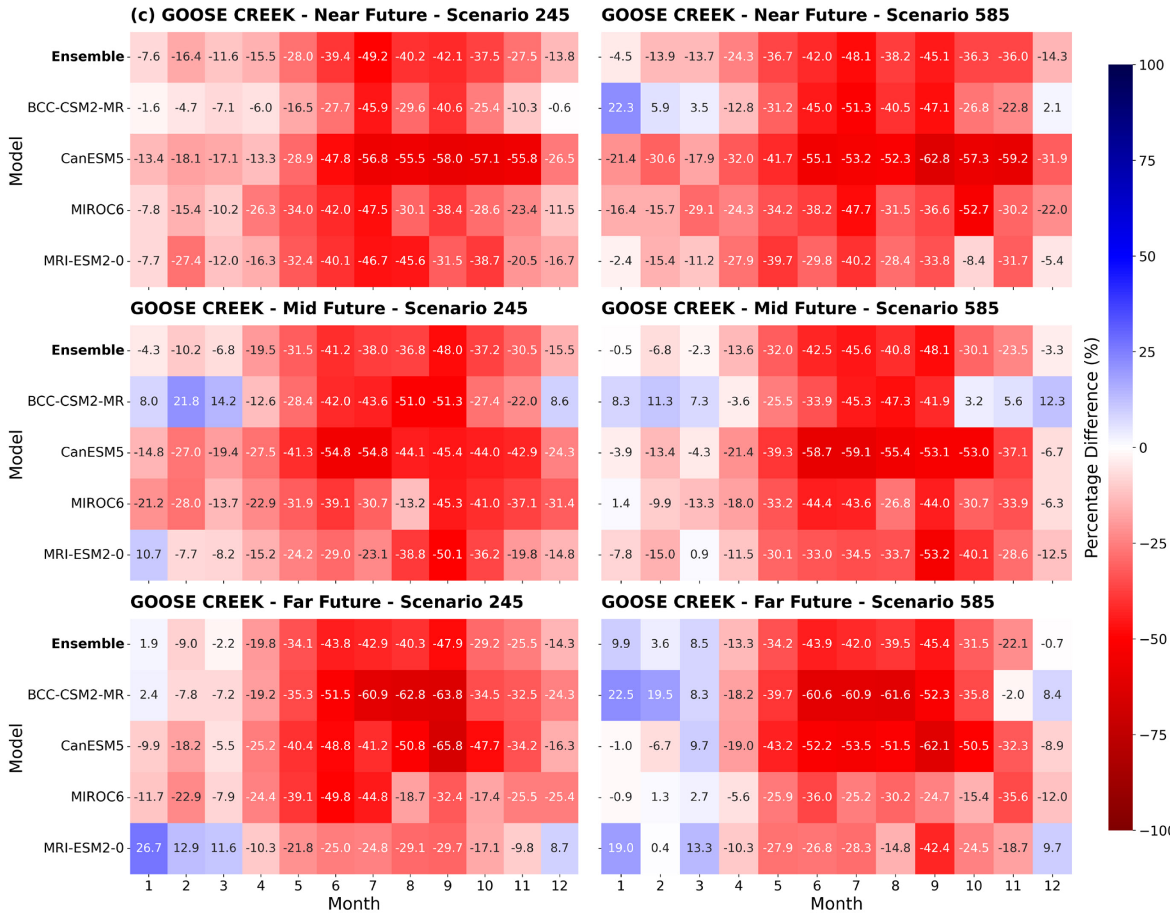

Fig. 5. The average monthly streamflow difference in percentage between the historical and GCMs at (a) Tarboro station, (b) Washington, and (c) Goose Creek Game Land station over the near future (2024-2044), mid future (2045-2069), and far future (2070-2100) under the SPP2-45 and 5-85 scenarios. Darker colors represent higher values.

Figure 5 shows the average monthly streamflow differences, in percentages, between historical period (2003-2019) and GCMs for the near future (2024-2044), mid future (2045-2069), and far future (2070-2100) under the SSP2-45 and 5-85 scenarios. In general, in these regions, the winter months (December to March) are expected to experience higher streamflow compared to other seasons (Fig. 5) while the summer period (May to October) is projected to be drier. Besides, as we approach the year 2100, the contrast between the wetter and drier months becomes more marked as a high discrepancy over the examined regions. It means the projected wet months are expected to be significantly wetter, while the dry months become increasingly drier especially under the SSP5-85 scenario.

3.5. Future changes in drought

In the previous section, we evaluated projected future floods. However, quantifying drought events both statistically and spatially is equally important. In this section, we utilize the 12-month drought index (SPI-12) (see Section 2.6) to measure drought intensity and frequency. Specifically, the SPI-12 index is calculated using projected future precipitation data from various GCMs and the ensemble model under different SSP scenarios, across the Tar-Pamlico River basin (Fig. 6 and Table 6). In general, a drying trend is observed during the near future (2024-2044), but the basin trends towards wetter conditions with an increased risk of flooding as we approach 2100 (Fig. 6, Tables 4 and 5). Under the SSP2-45 scenario, a transition to wetter conditions is found by 2100.

The Tar-Pamlico River basin exhibits dry conditions ($\overline{SPI12^{2-45}_{near}}$ = – 0.154) during the near future period, then becomes wetter ($\overline{SPI12^{2-45}_{mid}}$ = + 0.048), and reaching its peak wetness in the far future ($\overline{SPI12^{2-45}_{far}}$ = + 0.097) (Fig. 6 and Table 6). This trend is projected to occur across the examined regions and intensifies under the impacts of the SSP5-85 scenario. Specifically, the driest conditions are forecasted with ($\overline{SPI12^{5-85}_{near}}$ = – 0.602), while a significantly wetter trend is indicated for the far future under SSP5-85 ($\overline{SPI12^{2-45}_{far}}$ = + 0.445). These results confirm that higher emission projections not only have more substantial impacts but also contribute significantly to increased variability between seasons and throughout the future periods. Similarly, the Tarboro, Washington, and Goose Creek Game Land regions are projected to experience dry conditions in the near future (2024-2044) and become wetter in the mid- and far-future periods, with the SSP5-85 scenario showing a more pronounced intensity of these conditions (Table 6).

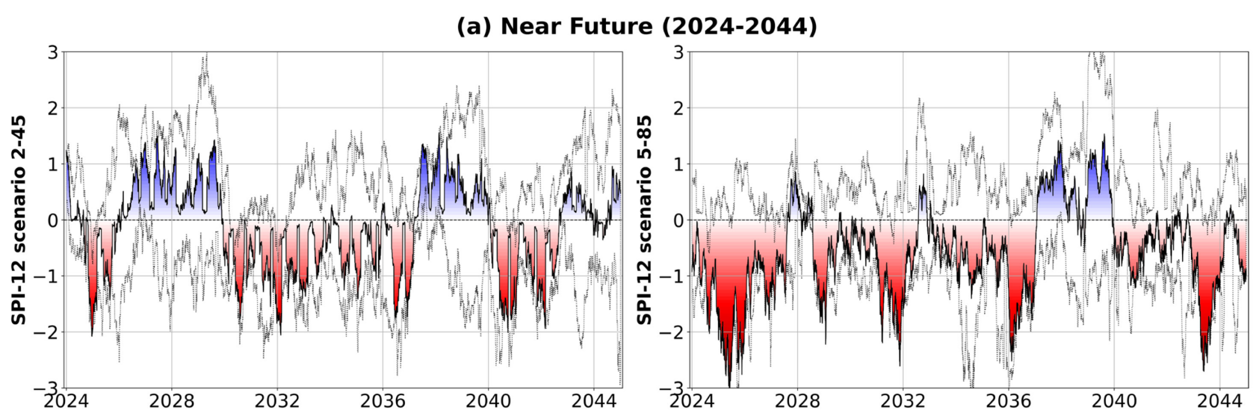

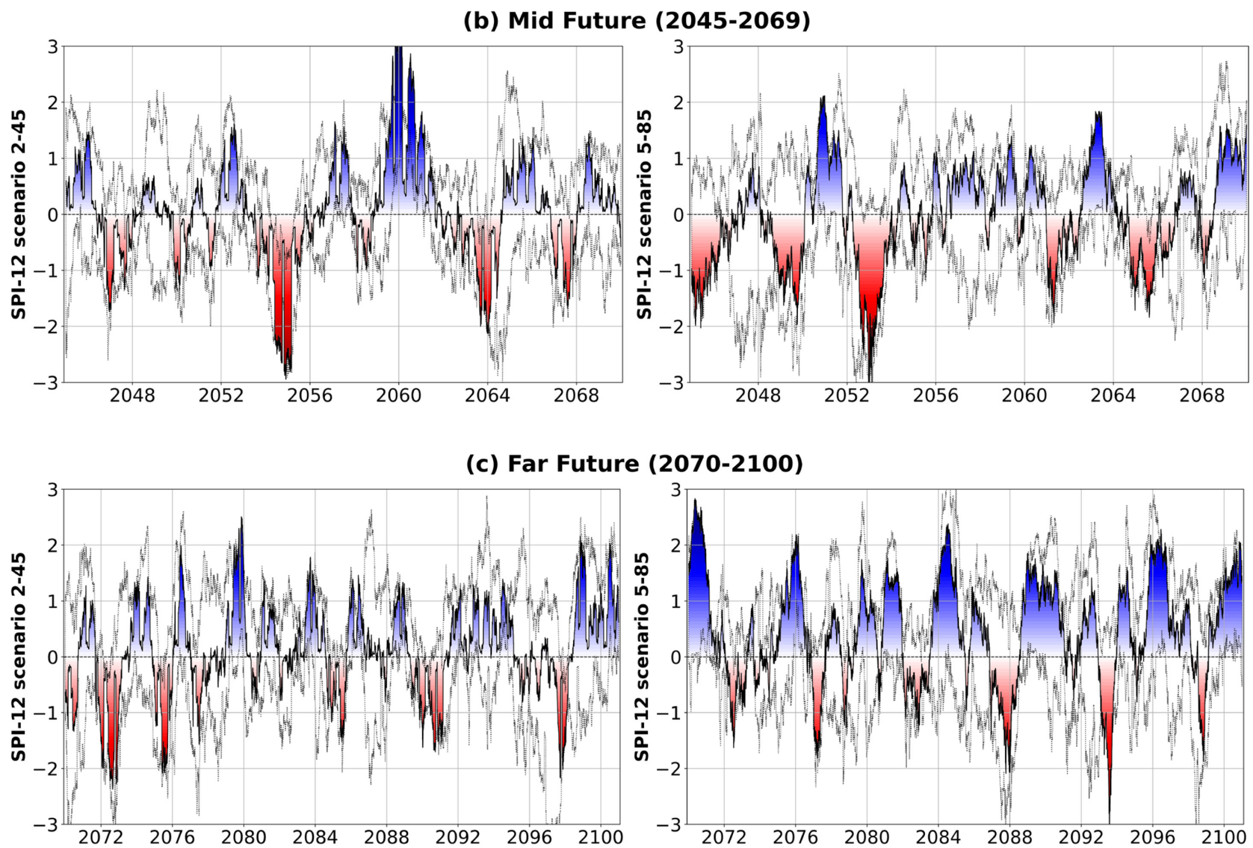

Fig. 6. Evaluation of droughts using SPI-12 index for the (a) near future (2024-2044), (b) mid future (2045-2069), and (c) far future (2070-2100) under SSP2-45 and 5-85 scenarios. Red color indicates dry periods, while the blue color signifies wet periods. The drought severity classification is presented in Table 4. Black dotted line represents the SPI-12 range across different GCMs, whereas the red and blue colors denote the values of the ensemble model.

Table 6.

Summary of the average SPI-12 index for the Tarboro, Washington, Goose Creek Game Land, and the entire Tar-Pamlico River basin from different GCMs, the ensemble model, and their SPPs across the near future (2024-2044), mid future (2045-2069), and far future (2070-2100). Positive (+) values, indicated in blue, suggest a wet trend, while negative (–) values, shown in red, denote a dry trend. The severity ranges for the SPI-12 drought index can be found in Table 4.

Site	**Ensemble model (SSP2-45)**		
	Near future (2024-2044)	Mid future (2045-2069)	Far future (2070-2100)
Tarboro	– 0.141	+ 0.058	+ 0.111
Washington	– 0.159	+ 0.068	+ 0.067
Goose Creek	– 0.159	+ 0.068	+ 0.067

Tar-Pamlico	– 0.154	+ 0.048	+ 0.097
	Ensemble model (SSP5-85)		
	Near future (2024-2044)	Mid future (2045-2069)	Far future (2070-2100)
Tarboro	– 0.592	– 0.048	+ 0.426
Washington	– 0.568	– 0.034	+ 0.412
Goose Creek	– 0.568	– 0.034	+ 0.412
Tar-Pamlico	– 0.602	– 0.045	+ 0.445

On the other hand, we have spatially quantified the magnitude and frequency of projected future droughts over the near future, mid future, and far future within the Tar-Pamlico River basin. This aims to better understand how climatic extremes could impact regions that are either rapidly developing or inherently at risk due to their low-lying nature.

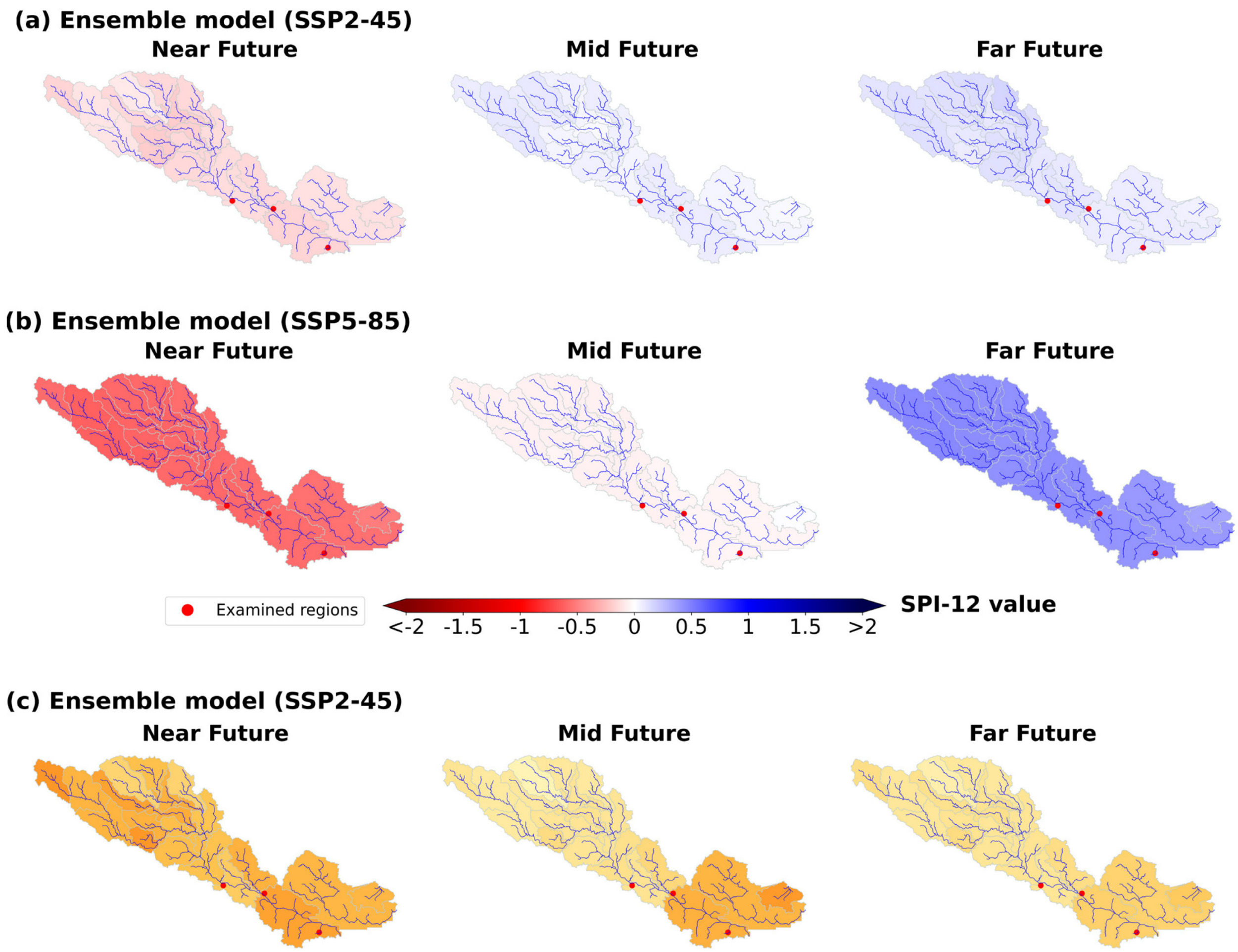

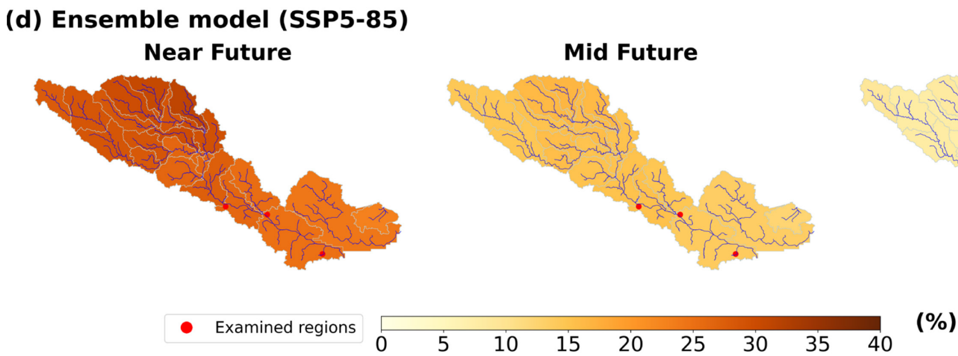

Fig. 7. Spatial distribution of drought using SPI-12 index over different GCMs and the ensemble model in three different time periods, including near future (2024-2044), mid future (2045-2069), and far future (2070-2100). The blue color represents the wet trend while the red color represents the dry trend. In this, (a) and (c) represent the results from the ensemble model for the SSP2-45 scenario while (b) and (d) represent the probability of drought occurrence (%) from the ensemble model for the SSP5-85 scenario.

Figure 7 shows the spatial distribution of drought intensity using the SPI-12 index across various GCMs and the ensemble model for three different periods: the near future (2024-2044), mid future (2045-2069), and far future (2070-2100). The Tar-Pamlico River basin as well as Tarboro, Washington, and Goose Creek Game Land are found to become wetter, reaching peak wetness during the far future, while the 2020s-2040s are expected to exhibit drier conditions (Figs. 7a and 7b). We found that higher emission scenarios indicating more severe impacts for drought and flood events throughout future periods. Moreover, there is a noticeable correlation between drought intensity and frequency within the basin, with low-lying (i.e., Washington; S2) and coastal regions (i.e., Goose Creek Game Land; S3), as downstream regions, are likely to experience a greater number of drought events between 2024 and 2100 compared to higher altitude regions (i.e., Tarboro; S1) (Figs. 7c and 7d). Indeed, toward 2100, the Tar-Pamlico River basin as well as these regions are likely to experience wetter conditions, thus showing a lower probability of drought occurrence (Figs. 7c and 7d).

4. Discussion

We have revealed our findings in residential analysis (1990-2020) (see Section 3.1) along with the projected changes in meteorological conditions and their impact on future climatic extreme events (2024-2100) over the Tarboro, Washington, and Goose Creek Game Land regions of the Tar-Pamlico River basin (see Sections 3.3 to 3.5). In this section, we will provide our in-depth discussions on these findings and estimated trends for upcoming decades.

When examining the historical residential expansions, we found an increase in population since 2010 for the town of Tarboro and since 2000 for the city of Washington (Fig. 1). However, the growth in the number of housing units has been even more pronounced, with increases ranging from fivefold to approximately sixteenfold since 1990 (Fig. 1). Besides, this decade is projected to experience an approximate 40% rise (in 2020 compared to 2010) in both population and population density across the entire Tar-Pamlico River basin (Fig. 1), a trend likely to be accelerated as partly highlighted by the current urbanization rate in the United States (Center for Sustainable Systems, 2023). In addition, according to the 2020 Census data, the urban population in the United States increased by 6.4% between 2010 and 2020 (U.S. Census Bureau, 2022) and this trend was also highlighted at the state level. Within this study of the Tar-Pamlico River basin, the North Carolina's population is projected to reach approximately 13 million by 2040 (John, 2024) and 14 million by 2050 (Michael, 2022; U.S. Census Bureau, 2020), positioning it as the seventh most populous state, behind only California, Texas, Florida, New York, Pennsylvania, and Georgia (Michael, 2023, 2022). By 2050, it is projected that 89% of the U.S. population will reside in urban areas (UN Population Division, 2018). In the Tar-Pamlico region, the largest metropolitan areas are expected to see faster population growth compared to smaller municipalities and rural areas (Michael, 2023). Within this study, given the numerous factors that could interact and influence changes in this region's population, potentially exacerbating or mitigating the intensity of climatic extremes toward 2100, we have provided the analyses mentioned above as our estimations of future trends and recommend using them as references to support regional adaptive measures but not as definitive statements.

In this study, we observed an increase in temperature and rainfall across seasons and various future periods, with a more likely pronounced difference in the intensity of climatic extremes (Figs. 5 and 6). To be specific, the near future is expected to experience more severe impacts from drought, whereas the mid and far future periods are likely to see increased flooding impacts (Figs. 4, 5, and 6). The summer season (May to October) is projected to be drier, especially during the near future (Table 6). This condition would then increase the region's vulnerability to extreme heat and could adversely affect agricultural activities. Conversely, the far future is predicted to be highly prone to flooding (Fig. 6) in which this could cause more water-related issues in terms of water sanitation and hygiene. We found that higher intensity and frequency of climatic extremes are associated with more severe greenhouse gas emissions (SSP5-85). Indeed, an increase in flood peaks of between 3 and 7% is observed during the mid-future period with a potential rise up to 21% in the far future period compared to the historical period (2003-2019) (Fig. 3). Besides, the mid- and far-future periods are projected to exhibit significant discrepancies between dry and wet seasons, highlighting substantial damage to agriculture and human activities that are caused by seasonal changes in meteorological conditions (Fig. 5). Downstream regions are expected to experience severe droughts with reduced rainfall during the summer season throughout the near future compared to higher altitude regions.

Besides, low-lying and coastal regions are likely to face higher flood intensities in terms of flood peaks (Figs. 3 and 5). Besides, when examining the probability of drought occurrence in this region, it appears that both low-lying and coastal areas are likely to experience more frequent drought events compared to other areas.

In our analysis, as temperatures would rapidly rise toward 2100 (Table 5) as well as the summer season tends to exhibit severe dryness, the demand for air conditioning and refrigeration is anticipated to increase, leading to higher energy consumption (Li et al., 2019). This not only places a burden on electrical grids, potentially causing outages during heatwaves but also escalates energy costs, impacting household and business finances (Chen et al., 2021). Extreme temperatures can also decrease economic productivity (e.g., agriculture), particularly in physically demanding jobs (Kjellstrom et al., 2009; Tran et al., 2024), and discourage outdoor activities, such as shopping and dining, thereby affecting businesses dependent on pedestrian patronage. Besides, previous studies have indicated a correlation between socioeconomic activities, population changes, and extreme events (Ahmadalipour et al., 2019; Bahinipati and Venkatachalam, 2016). If the total number of concrete-based infrastructures such as housing units continue to increase (as the current trend found in this study; see Section 3.1), it can significantly intensify impacts of natural hazards due to the increase the impervious surface area (Zhang et al., 2013). In this point, we expected for a correlation found as projected changes in climate extremes under impacts of increasing housing units that could be revealed using future projected LULC maps. Furthermore, this could lead to the increase of health-related issues due to higher urban heat (Nguyen et al., 2022; Yin et al., 2018; Zhou and Chen, 2018), especially for the elderly (Zhang et al., 2019) and children (Faurie et al., 2022). Besides, higher urban temperatures can exacerbate air pollution by increasing the rate of chemical reactions that produce pollutants, such as ozone (Li et al., 2018; Ulpiani, 2021), suggesting a need for adaptive measures to reduce this increasing trend over the Tar-Pamlico River basin.

On the other hand, agriculture in urban and peri-urban areas over in the Tar-Pamlico region may experience reduced crop yields due to heat stress on plants and livestock (Lwasa et al., 2014). These changes disproportionately impact low-income communities that often rely on agriculture and those living in densely populated areas with limited green spaces (Chakraborty et al., 2019), thereby leading to exacerbated social inequalities (Darrel Jenerette et al., 2011). Consequently, our findings highlight the significant potential for these severe problems to become worsen toward 2100. Therefore, it is crucial for authorities and stakeholders in the Tar-Pamlico River basin to implement sustainable management practices to mitigate the impacts of climate change.

4. Limitations and future works

In this work, we acknowledge our limitations, in which we have not included projected future changes in residential expansions (housing units and density) and population up to 2100. Additionally, incorporating more GCM candidates could reduce uncertainties and better quantify the variability of climatic extremes using future climate projections in hydrological models. Besides, it is beneficial to involve regional downscaling and bias correction of these GCMs before utilizing. For future work, we plan to reduce these limitations as well as integrate our model with other models, such as the Regional Ocean Modeling System (ROMS) to explore how the effects of sea-level rise and estuarine salinity might be exacerbated under the impacts of climate change (Yin et al., 2024) which is important for the Tar-Pamlico River basin. Our primary objective is to deliver more accurate and useful outcomes to support the decision-making of this region.

5. Conclusions

In this work, we conducted a comprehensive analysis to quantify the anticipated changes in future extremes using the NASA NEX-GDDP-CMIP6 dataset, along with regional residential expansions and LULC changes for the Tar-Pamlico River basin, North Carolina. Specifically, our work investigated the impacts of two future greenhouse gas emission scenarios, SSP2-45 and 5-85, for the region between 2024 and 2100. Our results revealed projected changes in meteorological conditions and their impacts on future climatic extreme events, while also discussing estimated impacts on the region. Key findings are summarized:

(1) A notable increasing trend is expected in meteorological conditions, with higher intensity and frequency of climatic extremes associated with more severe greenhouse gas emissions. Flood peaks are projected to increase between 3 and 7% during the mid-future period and could rise to 21% in the far future period compared to the historical period. Additionally, climatic extremes are projected to occur more frequently and likely to intensify and become more severe due to residential expansions.
(2) The near future is expected to experience more severe impacts from drought, whereas the mid- and far-future periods are likely to see increased flooding impacts. Besides, these periods also exhibit significant discrepancies between dry and wet seasons, highlighting substantial damage caused by seasonal changes, especially to agriculture.
(3) Downstream regions are expected to experience severe droughts with reduced rainfall during the summer season throughout the near future, compared to high altitude regions. Additionally, low-lying and coastal areas are likely to be more vulnerable as they are expected to face higher flood intensities, particularly in terms of peaks, as well as more frequent drought events compared to other areas.

Our work provide a scientific basis for quantifying the impact of future climate changes on the region’s water resources. Our approach, which incorporates regional characteristics along with hydrological analyses, shows potential to better highlight insights to support the long term resilience and safety of the region against the challenges posed by climate change. Consequently, this work serves as a valuable resource for stakeholders and authorities, assisting them in planning of sustainable strategies focused on natural disaster prevention and management.

CRediT authorship contribution statement

Thanh-Nhan-Duc Tran: Conceptualization, Methodology, Data curation, Software, Validation, Investigation, Formal analysis, Visualization, Writing – original draft, Writing – review & editing. **Mahesh R Tapas**: Software, Data curation, Validation, Writing – review & editing. **Son K. Do**: Writing – review & editing. **Randall Etheridge**: Writing – review & editing. **Venkataraman Lakshmi**: Writing – review & editing, Supervision.

Data availability

Data will be made available on request.

Declaration of competing interest

The authors declare that they have no known competing financial interests or personal relationships that could have appeared to influence the work reported in this paper.

Acknowledgments

We want to express our special thanks to the reviewers for their insightful and constructive comments. This work supports the Focused Coastlines and People (CoPe): Building Capacity for Adaptation in Rural Coastal Communities for the Eastern Shore of Virginia, Virginia, United States, and is funded by the National Science Foundation (NSF) under Grant No. 2052889 under the collaboration between the University of Virginia (Virginia) and the East Carolina University (North Carolina), United States.

References

Ahmadalipour, A., Moradkhani, H., Castelletti, A., Magliocca, N., 2019. Future drought risk in Africa: Integrating vulnerability, climate change, and population growth. Science of the Total Environment 662, 672–686. https://doi.org/10.1016/j.scitotenv.2019.01.278

Ahmed, Z., Tran, T.N.D., Nguyen, Q.B., 2020. Applying semi distribution hydrological model SWAT to assess hydrological regime in Lai Giang catchment, Binh Dinh Province, Vietnam, in: Proceedings of the 2nd Conference on Sustainability in Civil Engineering (CSCE'20), Capital University of Science and Technology, Islamabad, Pakistan. p.8.

Anjanee Prabha, J., Tapas, M.R., 2020. Event-Based Rainfall-Runoff Modeling Using HEC-HMS. IOSR Journal of Mechanical and Civil Engineering (IOSR-JMCE) e-ISSN 17, 41–59. https://doi.org/10.9790/1684-1704034159

Arnold, J.G., Moriasi, D.N., Gassman, P.W., Abbaspour, K.C., White, M.J., Srinivasan, R., Santhi, C., Harmel, R.D., Van Griensven, A., Van Liew, M.W., Kannan, N., Jha, M.K., 2012. SWAT: Model use, calibration, and validation. Trans ASABE 55, 1491–1508. https://doi.org/10.13031/2013.42256

Arshad, A., Mirchi, A., Samimi, M., Ahmad, B., 2022. Combining downscaled-GRACE data with SWAT to improve the estimation of groundwater storage and depletion variations in the Irrigated Indus Basin (IIB). Science of the Total Environment 838, 156044. https://doi.org/10.1016/j.scitotenv.2022.156044

Arshad, A., Zhang, W., Zhang, Z., Wang, S., Zhang, B., Jehanzeb, M., Cheema, M., Jafari, M., 2021. Reconstructing high-resolution gridded precipitation data using an improved downscaling approach over the high altitude mountain regions of Upper Indus Basin (UIB). Science of the Total Environment 784, 147140. https://doi.org/10.1016/j.scitotenv.2021.147140

Aryal, A., Tran, T.N.D, Kumar, B., Lakshmi, V., 2023. Evaluation of Satellite-Derived Precipitation Products for Streamflow Simulation of a Mountainous Himalayan Watershed: A Study of Myagdi Khola in Kali Gandaki. Remote Sens (Basel) 15, 47–62. https://doi.org/10.3390/rs15194762

Ashrafi, S., Kerachian, R., Pourmoghim, P., Behboudian, M., Motlaghzadeh, K., 2022a. Evaluating and improving the sustainability of ecosystem services in river basins under climate change. Science of the Total Environment 806. https://doi.org/10.1016/j.scitotenv.2021.150702

Ashrafi, S., Khoie, M.M.M., Kerachian, R., Shafiee-Jood, M., 2022b. Managing basin-wide ecosystem services using the bankruptcy theory. Science of the Total Environment 842. https://doi.org/10.1016/j.scitotenv.2022.156845

Aslam, R.A., Shrestha, S., Usman, M.N., Khan, S.N., Ali, S., Sharif, M.S., Sarwar, M.W., Saddique, N., Sarwar, A., Ali, M.U., Arshad, A., 2022. Integrated SWAT-MODFLOW Modeling-Based Groundwater Adaptation Policy Guidelines for Lahore , Pakistan under Projected Climate Change , and Human Development Scenarios. Atmosphere (Basel) 13, 2001. https://doi.org/10.3390/atmos13122001

Bahinipati, C.S., Venkatachalam, L., 2016. Role of climate risks and socio-economic factors in influencing the impact of climatic extremes: a normalisation study in the context of Odisha, India. Reg Environ Change 16, 177–188. https://doi.org/10.1007/s10113-014-0735-4

Baills, A., Garcin, M., Bulteau, T., 2020. Assessment of selected climate change adaptation measures for coastal areas. Ocean Coast Manag 185. https://doi.org/10.1016/j.ocecoaman.2019.105059

Behboudian, M., Kerachian, R., Motlaghzadeh, K., Ashrafi, S., 2021. Evaluating water resources management scenarios considering the hierarchical structure of decision-makers and ecosystem services-based criteria. Science of the Total Environment 751. https://doi.org/10.1016/j.scitotenv.2020.141759

Bieger, K., Arnold, J.G., Rathjens, H., White, M.J., Bosch, D.D., Allen, P.M., Volk, M., Srinivasan, R., 2017. Introduction to SWAT+, a completely restructured version of the soil and water assessment tool. JAWRA Journal of the American Water Resources Association 53, 115–130. https://doi.org/10.1111/1752-1688.12482

Blasone, R.-S., Vrugt, J.A., Madsen, H., Rosbjerg, D., Robinson, B.A., Zyvoloski, G.A., 2008. Generalized likelihood uncertainty estimation (GLUE) using adaptive Markov Chain Monte Carlo sampling. Adv Water Resour 31, 630–648. https://doi.org/10.1016/j.advwatres.2007.12.003

Bonsoms, J., Oliva, M., Alonso-González, E., Revuelto, J., López-Moreno, J.I., 2023. Impact of climate change on snowpack dynamics in coastal Central-Western Greenland. Science of The Total Environment 169616. https://doi.org/10.1016/j.scitotenv.2023.169616

Cao, K., Liu, X., Fu, Q., Wang, Y., Liu, D., Li, T., Li, M., 2023. Dynamic and harmonious allocation of irrigation water resources under climate change: A SWAT-based multi-objective nonlinear framework. Science of the Total Environment 905. https://doi.org/10.1016/j.scitotenv.2023.167221

Carter, T.R., Parry, M.L., Harasawa, H., Nishioka, S., 1994. IPCC Technical Guidelines for Assessing Climate Change Impacts and Adaptations. Radioative Forcing of Climate Change; Evaluation of the IPCC IS92 Emission Scenarios and the IPCC Guidelines for Nacional Greenshouse Gas Inventories.

Center for Sustainable Systems, University of Michigan. 2023. “U.S. Cities Factsheet.” Pub. No. CSS09-06. No volume.

Chakraborty, T., Hsu, A., Manya, D., Sheriff, G., 2019. Disproportionately higher exposure to urban heat in lower-income neighborhoods: A multi-city perspective. Environmental Research Letters. https://doi.org/10.1088/1748-9326/ab3b99

Chen, C., Gan, R., Feng, D., Yang, F., Zuo, Q., 2022. Quantifying the contribution of SWAT modeling and CMIP6 inputting to streamflow prediction uncertainty under climate change. J Clean Prod 364, 132675. https://doi.org/10.1016/j.jclepro.2022.132675

Chen, Y., Liu, A., Cheng, X., 2020. Quantifying economic impacts of climate change under nine future emission scenarios within CMIP6. Science of the Total Environment 703. https://doi.org/10.1016/j.scitotenv.2019.134950

Cheng, X., Chen, L., Sun, R., Kong, P., 2018. Land use changes and socio-economic development strongly deteriorate river ecosystem health in one of the largest basins in China. Science of the Total Environment 616–617, 376–385. https://doi.org/10.1016/j.scitotenv.2017.10.316

Cole, M.B., Augustin, M.A., Robertson, M.J., Manners, J.M., 2018. The science of food security. NPJ Sci Food 2. https://doi.org/10.1038/s41538-018-0021-9

Darrel Jenerette, G., Harlan, S.L., Stefanov, W.L., Martin, C.A., 2011. Ecosystem services and urban heat riskscape moderation: Water, green spaces, and social inequality in Phoenix, USA. Ecological Applications 21, 2637–2651. https://doi.org/10.1890/10-1493.1

Donnelly, J., Daneshkhah, A., Abolfathi, S., 2024a. Forecasting global climate drivers using Gaussian processes and convolutional autoencoders. Eng Appl Artif Intell 128. https://doi.org/10.1016/j.engappai.2023.107536

Donnelly, J., Daneshkhah, A., Abolfathi, S., 2024b. Physics-informed neural networks as surrogate models of hydrodynamic simulators. Science of the Total Environment 912. https://doi.org/10.1016/j.scitotenv.2023.168814

Di Virgilio, G., Ji, F., Tam, E., Nishant, N., Evans, J.P., Thomas, C., Riley, M.L., Beyer, K., Grose, M.R., Narsey, S., Delage, F., 2022. Selecting CMIP6 GCMs for CORDEX Dynamical Downscaling: Model Performance, Independence, and Climate Change Signals. Earths Future 10. https://doi.org/10.1029/2021EF002625

Dias, C.G., Martins, F.B., Martins, M.A., 2024. Climate risks and vulnerabilities of the Arabica coffee in Brazil under current and future climates considering new CMIP6 models. Science of the Total Environment 907. https://doi.org/10.1016/j.scitotenv.2023.167753

Dile, Y., Srinivasan, R., George, C., 2019. QGIS Interface for SWAT+(QSWAT+), version 1.2. 2, Texas AM University.

Douglas-Mankin, K.R., Srinivasan, R., Arnold, J.G., 2010. Soil and water assessment tool (SWAT) model: Current developments and applications. Trans ASABE 53, 1423–1431. https://doi.org/10.13031/2013.34915

Easterling, D.R., Meehl, G.A., Parmesan, C., Changnon, S.A., Karl, T.R., Mearns, L.O., 2000. Climate Extremes: Observations, Modeling, and Impacts 289, 2068–2075. https://doi.org/10.1126/science.289.5487.2068

Eyring, V., Bony, S., Meehl, G.A., Senior, C.A., Stevens, B., Stouffer, R.J., Taylor, K.E., Dynamique, D.M., Pierre, I., Laplace, S., Ipsl, L.M.D., 2016. Overview of the Coupled Model Intercomparison Project Phase 6 (CMIP6) experimental design and organization. Geosci Model Dev 9, 1937–1958. https://doi.org/10.5194/gmd-9-1937-2016

Faurie, C., Varghese, B.M., Liu, J., Bi, P., 2022. Association between high temperature and heatwaves with heat-related illnesses: A systematic review and meta-analysis. Science of the Total Environment. https://doi.org/10.1016/j.scitotenv.2022.158332

Garner, A.J., Mann, M.E., Emanuel, K.A., Kopp, R.E., Lin, N., Alley, R.B., Horton, B.P., DeConto, R.M., Donnelly, J.P., Pollard, D., 2017. Impact of climate change on New York City's coastal flood hazard: Increasing flood heights from the preindustrial to 2300 CE. Proc Natl Acad Sci U S A 114, 11861–11866. https://doi.org/10.1073/pnas.1703568114

Gopalakrishnan, T., Hasan, M.K., Haque, A.T.M.S., Jayasinghe, S.L., Kumar, L., 2019. Sustainability of coastal agriculture under climate change. Sustainability (Switzerland) 11. https://doi.org/10.3390/su11247200

Guan, X., Zhang, J., Bao, Z., Liu, C., Jin, J., Wang, G., 2021. Past variations and future projection of runoff in typical basins in 10 water zones, China. Science of the Total Environment 798. https://doi.org/10.1016/j.scitotenv.2021.149277

Gupta, H. V., Kling, H., Yilmaz, K.K., Martinez, G.F., 2009. Decomposition of the mean squared error and NSE performance criteria: Implications for improving hydrological modelling. J Hydrol (Amst) 377, 80–91. https://doi.org/10.1016/j.jhydrol.2009.08.003

Hansen, G., Stone, D., 2016. Assessing the observed impact of anthropogenic climate change. Nat Clim Chang 6, 532–537. https://doi.org/10.1038/nclimate2896

Hsiao, S.C., Chiang, W.S., Jang, J.H., Wu, H.L., Lu, W.S., Chen, W.B., Wu, Y.T., 2021. Flood risk influenced by the compound effect of storm surge and rainfall under climate change for low-lying coastal areas. Science of the Total Environment 764. https://doi.org/10.1016/j.scitotenv.2020.144439

IPCC, 2021. Climate Change 2021: The Physical Science Basis. Contribution of Working Group I to the Sixth Assessment Report of the Intergovernmental Panel on Climate Change.

IPCC, 2019. Global warming of 1.5°C, Special Report on Global Warming of 1.5°C.

IPCC, 2013. Climate Change 2013—The Physical Science Basis, Chemistry International. https://doi.org/10.1515/ci-2021-0407

IPPC, 2021. Chapter Outline of The Working Group III Contribution To The IPCC Six Assessment Report (AR6).

Kang, H., Sridhar, V., Ali, S.A., 2022. Climate change impacts on conventional and flash droughts in the Mekong River Basin. Science of the Total Environment 838. https://doi.org/10.1016/j.scitotenv.2022.155845

Keith, D.J., 2014. Satellite remote sensing of chlorophyll a in support of nutrient management in the Neuse and Tar-Pamlico River (North Carolina) estuaries. Remote Sens Environ 153, 61–78. https://doi.org/10.1016/j.rse.2014.05.019

Kjellstrom, T., Holmer, I., Lemke, B., 2009. Workplace heat stress, health and productivity-an increasing challenge for low and middle-income countries during climate change. Glob Health Action 2. https://doi.org/10.3402/gha.v2i0.2047

Li, H., Meier, F., Lee, X., Chakraborty, T., Liu, J., Schaap, M., Sodoudi, S., 2018. Interaction between urban heat island and urban pollution island during summer in Berlin. Science of the Total Environment 636, 818–828. https://doi.org/10.1016/j.scitotenv.2018.04.254

Li, X., Zhou, Y., Yu, S., Jia, G., Li, H., Li, W., 2019. Urban heat island impacts on building energy consumption: A review of approaches and findings. Energy. https://doi.org/10.1016/j.energy.2019.02.183

Lien, M.K., 2019. Vulnerability Assessment of Climate Change on Sea Level Rise Impacts on Some Economic Sectors in Binh Dinh Province, Vietnam. Am J Clim Change 08, 302–324. https://doi.org/10.4236/ajcc.2019.82017

Liu, C., Yang, C., Yang, Q., Wang, J., 2021. Spatiotemporal drought analysis by the standardized precipitation index (SPI) and standardized precipitation evapotranspiration index (SPEI) in Sichuan Province, China. Sci Rep 11, 1–14. https://doi.org/10.1038/s41598-020-80527-3

Loc, H.H., Van Binh, D., Park, E., Shrestha, S., Dung, T.D., Son, V.H., Truc, N.H.T., Mai, N.P., Seijger, C., 2021. Intensifying saline water intrusion and drought in the Mekong Delta: From physical evidence to policy outlooks. Science of the Total Environment 757. https://doi.org/10.1016/j.scitotenv.2020.143919

Lwasa, S., Mugagga, F., Wahab, B., Simon, D., Connors, J., Griffith, C., 2014. Urban and peri-urban agriculture and forestry: Transcending poverty alleviation to climate change mitigation and adaptation. Urban Clim 7, 92–106. https://doi.org/10.1016/j.uclim.2013.10.007

Ma, F., Yuan, X., 2021. Impact of climate and population changes on the increasing exposure to summertime compound hot extremes. Science of the Total Environment 772. https://doi.org/10.1016/j.scitotenv.2021.145004

Mafi-Gholami, D., Jaafari, A., Zenner, E.K., Nouri Kamari, A., Tien Bui, D., 2020. Vulnerability of coastal communities to climate change: Thirty-year trend analysis and prospective prediction for the coastal regions of the Persian Gulf and Gulf of Oman. Science of the Total Environment 741. https://doi.org/10.1016/j.scitotenv.2020.140305

Mahdian, M., Hosseinzadeh, M., Siadatmousavi, S.M., Chalipa, Z., Delavar, M., Guo, M., Abolfathi, S., Noori, R., 2023. Modelling impacts of climate change and anthropogenic activities on inflows and sediment loads of wetlands: case study of the Anzali wetland. Sci Rep 13. https://doi.org/10.1038/s41598-023-32343-8

Mahdian, M., Noori, R., Salamattalab, M.M., Heggy, E., Bateni, S.M., Nohegar, A., Hosseinzadeh, M., Siadatmousavi, S.M., Fadaei, M.R., Abolfathi, S., 2024. Anzali Wetland Crisis: Unraveling the Decline of Iran's Ecological Gem. Journal of Geophysical Research: Atmospheres 129. https://doi.org/10.1029/2023JD039538

Mapes, K.L., Pricope, N.G., 2020. Evaluating SWAT model performance for runoff, percolation, and sediment loss estimation in low-gradient watersheds of the Atlantic Coastal Plain. Hydrology 7. https://doi.org/10.3390/HYDROLOGY7020021

Masciopinto, C., Liso, I.S., 2016. Assessment of the impact of sea-level rise due to climate change on coastal groundwater discharge. Science of the Total Environment 569–570, 672–680. https://doi.org/10.1016/j.scitotenv.2016.06.183

Maurer, E.P., Hidalgo, H.G., 2008. Utility of daily vs. monthly large-scale climate data: an intercomparison of two statistical downscaling methods. Hydrol Earth Syst Sci 12, 551–563. https://doi.org/10.5194/hess-12-551-2008

Maurer, E.P., Kayser, G., Doyle, L., Wood, A.W., 2018. Adjusting Flood Peak Frequency Changes to Account for Climate Change Impacts in the Western United States. J Water Resour Plan Manag 144. https://doi.org/10.1061/(asce)wr.1943-5452.0000903

Merz, B., Basso, S., Fischer, S., Lun, D., Blöschl, G., Merz, R., Guse, B., Viglione, A., Vorogushyn, S., Macdonald, E., Wietzke, L., Schumann, A., 2022. Understanding Heavy Tails of Flood Peak Distributions. Water Resour Res. https://doi.org/10.1029/2021WR030506

Meyer, L., 2015. IPCC Fifth Assessment Report Synthesis Report Key Messages.

Michael, C., 2023. North Carolina's Strong Population Growth Continues [WWW Document]. North Carolina Office of State Budget and Management. URL https://www.osbm.nc.gov/blog/2023/12/20/north-carolinas-strong-population-growth-continues (accessed 1.24.24). Page 1-1, No volume.

Michael, C., 2022. NC's Population to Reach 14.0 Million by 2050 [WWW Document]. North Carolina Office of State Budget and Management. URL https://www.osbm.nc.gov/blog/2022/12/30/ncs-population-reach-140-million-2050 (accessed 1.24.24).

Mirzaei, M., Huang, Y.F., El-Shafie, A., Shatirah, A., 2015. Application of the generalized likelihood uncertainty estimation (GLUE) approach for assessing uncertainty in hydrological models: a review. Stochastic environmental research and risk assessment 29, 1265–1273.

Mishra, G.J., Kumar, A.U., Tapas, M.R., Oggu, P., Jayakumar, K. V., 2023. Evaluating hydrological alterations and recommending minimum flow release from the Ujjani dam to improve the Bhima River ecosystem health. Water Science and Technology 88, 763–777. https://doi.org/10.2166/wst.2023.236

Moriasi, D.N., Gitau, M.W., Pai, N., Daggupati, P., 2015. Hydrologic and water quality models: Performance measures and evaluation criteria. Trans ASABE 58, 1763–1785. https://doi.org/10.13031/trans.58.10715

Mulligan, R.P., Mallinson, D.J., Clunies, G.J., Rey, A., Culver, S.J., Zaremba, N., Leorri, E., Mitra, S., 2019. Estuarine Responses to Long-Term Changes in Inlets, Morphology, and Sea Level Rise. J Geophys Res Oceans 124, 9235–9257. https://doi.org/10.1029/2018JC014732

Nash, J.E., Sutcliffe, J. V, 1970. River flow forecasting through conceptual models part I—A discussion of principles. J Hydrol (Amst) 10, 282–290. https://doi.org/10.1016/0022-1694(70)90255-6

NC DEQ, 2009. Final Neuse River Basin wide water quality plan. Raleigh. Page: 1-514. No volume.

NC DEQ, 1994. Tar-Pamlico River basin wide water quality management plan. Division of Environmental Management, Water Quality Section Raleigh, North Carolina. Page: 1-284. No volume.

NC Wildlife, 2018. Goose Creek Game Land Management Plan.

Neill, B.C.O., Tebaldi, C., Vuuren, D. Van, Eyring, V., Hurtt, G., Knutti, R., Kriegler, E., Lamarque, J., 2016. The Scenario Model Intercomparison Project (ScenarioMIP) for CMIP6. Geosci Model Dev 1–35. https://doi.org/10.5194/gmd-2016-84

Neitsch, S.L., Arnold, J.G., Kiniry, J.R., Williams, J.R., 2011. Soil & Water Assessment Tool Theoretical Documentation Version 2009. Texas Water Resources Institute 1–647. https://doi.org/10.1016/j.scitotenv.2015.11.063

Nguyen, B.Q., Kantoush, S.A., Tran, T.-N.-D., Binh, D. Van, Vo, N.D., Saber, M., Sumi, T., 2023. Response of Hydrological to Anthropogenic Activities in a Tropical Basin. pp. 269–278. https://doi.org/10.3850/978-90-833476-1-5_iahr40wc-p1339-cd

Nguyen, B.Q., Tran, T.N.D., Grodzka-Łukaszewska, M., Sinicyn, G., Lakshmi, V., 2022. Assessment of Urbanization-Induced Land-Use Change and Its Impact on Temperature, Evaporation, and Humidity in Central Vietnam. Water (Switzerland) 14. https://doi.org/10.3390/w14213367

Nguyen, T. V., Dietrich, J., Dang, T.D., Tran, D.A., Van Doan, B., Sarrazin, F.J., Abbaspour, K., Srinivasan, R., 2022. An interactive graphical interface tool for parameter calibration, sensitivity analysis, uncertainty analysis, and visualization for the Soil and Water Assessment Tool. Environmental Modelling and Software 156. https://doi.org/10.1016/j.envsoft.2022.105497

Noor, R., Arshad, A., Shafeeque, M., Liu, J., Baig, A., 2023. Combining APHRODITE Rain Gauges-Based Precipitation with Downscaled-TRMM Data to Translate High-Resolution Precipitation Estimates in the Indus Basin. Remote Sens (Basel) 15, 318. https://doi.org/10.3390/rs15020318

Noori, R., Maghrebi, M., Jessen, S., Bateni, S.M., Heggy, E., Javadi, S., Noury, M., Pistre, S., Abolfathi, S., AghaKouchak, A., 2023. Decline in Iran's groundwater recharge. Nat Commun 14. https://doi.org/10.1038/s41467-023-42411-2

O'Donoghue, S., Lehmann, M., Major, D., Major-Ex, G., Sutherland, C., Motau, A., Haddaden, N., Kibria, A.S., Costanza, R., Groves, C., Behie, A., Johnson, K., 2021. Adaptation to climate change in small coastal cities: The influence of development status on adaptation response. Ocean Coast Manag 211. https://doi.org/10.1016/j.ocecoaman.2021.105788

Omojola, A., Dettinger, M.D., Diego, S., 2012. Climate change and cities: first assessment report of the Urban Climate Change Research Network. Choice Reviews Online 49, 49-3876-49–3876. https://doi.org/10.5860/choice.49-3876

Osmond, D.L., Hoag, D.L.K., Luloff, A.E., Meals, D.W., Neas, K., 2015. Farmers' Use of Nutrient Management: Lessons from Watershed Case Studies. J Environ Qual 44, 382–390. https://doi.org/10.2134/jeq2014.02.0091

P. W. Gassman, M. R. Reyes, C. H. Green, J. G. Arnold, 2007. The Soil and Water Assessment Tool: Historical Development, Applications, and Future Research Directions. Trans ASABE 50, 1211–1250. https://doi.org/10.13031/2013.23637

Parajuli, R., Thoma, G., Matlock, M.D., 2019. Environmental sustainability of fruit and vegetable production supply chains in the face of climate change: A review. Science of the Total Environment. https://doi.org/10.1016/j.scitotenv.2018.10.019

Park, E., Loc, H.H., Van Binh, D., Kantoush, S., 2022. The worst 2020 saline water intrusion disaster of the past century in the Mekong Delta: Impacts, causes, and management implications. Ambio 51, 691–699. https://doi.org/10.1007/s13280-021-01577-z

Park, T., Hashimoto, H., Wang, W., Thrasher, B., Michaelis, A.R., Lee, T., Brosnan, I.G., Nemani, R.R., 2023. What Does Global Land Climate Look Like at 2°C Warming? Earths Future 11, 1–16. https://doi.org/10.1029/2022EF003330

Peng, S., Wang, C., Li, Z., Mihara, K., Kuramochi, K., Toma, Y., Hatano, R., 2023. Climate change multi-model projections in CMIP6 scenarios in Central Hokkaido, Japan. Sci Rep 13, 1–18. https://doi.org/10.1038/s41598-022-27357-7

Pignotti, G., Rathjens, H., Cibin, R., Chaubey, I., Crawford, M., 2017. Comparative analysis of HRU and grid-based SWAT models. Water (Switzerland) 9, 272. https://doi.org/10.3390/w9040272

Porter, J.R., Shu, E., Amodeo, M., Hsieh, H., Freeman, N., Chu, J., 2021. Community Flood Impacts and Infrastructure: Examining National Flood Impacts Using a High Precision Assessment Tool in the United States. Water (Basel) 13, 25–31. https://doi.org/https://doi.org/10.3390/w13213125

Raftery, A.E., Zimmer, A., Frierson, D.M.W., Startz, R., Liu, P., 2017. Less than 2 °c warming by 2100 unlikely. Nat Clim Chang 7, 637–641. https://doi.org/10.1038/nclimate3352

Ren, J., Wang, W., Wei, J., Li, H., Li, X., Liu, G., Chen, Y., Ye, S., 2023. Evolution and prediction of drought-flood abrupt alternation events in Huang-Huai-Hai River Basin, China. Science of the Total Environment 869. https://doi.org/10.1016/j.scitotenv.2023.161707

Rosenzweig, C., Neofotis, P., 2013. Detection and attribution of anthropogenic climate change impacts. Wiley Interdiscip Rev Clim Change 4, 121–150. https://doi.org/10.1002/wcc.209

Saadi, Z., Alias, N.E., Yusop, Z., Iqbal, Z., Houmsi, M.R., Houmsi, L.N., Ramli, M.W.A., Muhammad, M.K.I., 2024. Application of relative importance metrics for CMIP6 models selection in projecting basin-scale rainfall over Johor River basin, Malaysia. Science of the Total Environment 912. https://doi.org/10.1016/j.scitotenv.2023.169187

Saeedi, M., Kim, H., Nabaei, S., Brocca, L., Lakshmi, V., Mosaffa, H., 2022. A comprehensive assessment of SM2RAIN-NWF using ASCAT and a combination of ASCAT and SMAP soil moisture products for rainfall estimation. Science of the Total Environment 838. https://doi.org/10.1016/j.scitotenv.2022.156416

Sanjay Mankar, T., Mane, S., Mali, S.T., Tapas, M.R., 2020. Analysis and Development of Watershed for Ruikhed Village, Maharashtra-A Case Study. International Research Journal of Engineering and Technology. Page: 2265-2270. Volume 7. Issue 8.

Shafeeque, M., Hafeez, M., Sarwar, A., Arshad, A., Khurshid, T., 2023a. Quantifying future water saving potential under climate change and groundwater recharge scenarios in Lower Chenab Canal, Indus River Basin. Theor Appl Climatol. https://doi.org/10.1007/s00704-023-04621-y

Shafeeque, M., Luo, Y., Arshad, A., Muhammad, S., 2023b. Assessment of climate change impacts on glacio hydrological processes and their variations within critical zone. Natural Hazards 115, 2721–2748. https://doi.org/10.1007/s11069-022-05661-9

Song, Y.H., Chung, E.S., Shahid, S., 2022. Differences in extremes and uncertainties in future runoff simulations using SWAT and LSTM for SSP scenarios. Science of the Total Environment 838. https://doi.org/10.1016/j.scitotenv.2022.156162

Svoboda, M., Lecomte, D., Hayes, M., Heim, R., Gleason, K., Angel, J., Rippey, B., Tinker, R., Palecki, M., Stooksbury, D., Miskus, D., Stephens, S., 2002. THE DROUGHT MONITOR. Bull Am Meteorol Soc 1181–1190. https://doi.org/10.1175/1520-0477-83.8.1181

SWAT+, 2020. CHAPTER FILE.CIO SWAT + INPUT DATA : Variable name. Swat+ Input/Output File Documentation. Page: 1-222. No volume.

SWAT+, 2018. Inputs_Swatplus.

Tan, L., Zhang, X., Qi, J., Sun, D., Marek, G.W., Feng, P., Li, Baogui, Liu, D.L., Li, Baoguo, Srinivasan, R., Chen, Y., 2023. Assessment of the sustainability of groundwater utilization and crop production under optimized irrigation strategies in the North China Plain under future climate change. Science of the Total Environment 899. https://doi.org/10.1016/j.scitotenv.2023.165619

Tapas, M., Etheridge, J.R., Howard, G., Lakshmi, V.V., Tran, T.N.D., 2022a. Development of a Socio-Hydrological Model for a Coastal Watershed: Using Stakeholders' Perceptions, in: AGU Fall Meeting Abstracts. pp. H22O--0996.

Tapas, M.R., Kumar, U., Mogili, S., Jayakumar, K. V., 2022b. Development of multivariate integrated drought monitoring index (MIDMI) for Warangal region of Telangana, India. Journal of Water and Climate Change 13. https://doi.org/10.2166/wcc.2021.065

Tapas, M., Etheridge, J. R., Tran, T.-N.-D., Le, M.-H., Hinckley B., Lakshmi, V., 2023. Satellite-based rainfall datasets and autocalibration techniques' effects on SWAT+ flow prediction. September 19, 2023. https://doi.org/10.22541/au.169510515.57261841/v1

Tran, T.-N.-D., & Lakshmi, V., 2022. The land use changes impacts on socio-economic drivers and simulation of surface and groundwater in the Eastern Shore of Virginia, the United States. AGU Fall Meeting Abstracts, 2022, H42D-1270.

Tarboton, D.G., 2011. A tutorial for using TauDEM to delineate a single watershed.

Tebaldi, C., Debeire, K., Eyring, V., Fischer, E., Fyfe, J., Friedlingstein, P., Knutti, R., Lowe, J., O'Neill, B., Sanderson, B., Van Vuuren, D., Riahi, K., Meinshausen, M., Nicholls, Z., Tokarska, K., Hurtt, G., Kriegler, E., Meehl, G., Moss, R., Bauer, S., Boucher, O., Brovkin, V., Yhb, Y., Dix, M., Gualdi, S., Guo, H., John, J., Kharin, S., Kim, Y.H., Koshiro, T., Ma, L., Olivié, D., Panickal, S., Qiao, F., Rong, X., Rosenbloom, N., Schupfner, M., Séférian, R., Sellar, A., Semmler, T., Shi, X., Song, Z., Steger, C., Stouffer, R., Swart, N., Tachiiri, K., Tang, Q., Tatebe, H., Voldoire, A., Volodin, E., Wyser, K., Xin, X., Yang, S., Yu, Y., Ziehn, T., 2021. Climate model projections from the Scenario Model Intercomparison Project (ScenarioMIP) of CMIP6. Earth System Dynamics 12, 253–293. https://doi.org/10.5194/esd-12-253-2021

Thibeault, J.M., Seth, A., 2014. Changing climate extremes in the Northeast United States: observations and projections from CMIP5. Clim Change 127, 273–287. https://doi.org/10.1007/s10584-014-1257-2

Thrasher, B., Wang, W., Michaelis, A., Melton, F., Lee, T., Nemani, R., 2022. NASA Global Daily Downscaled Projections, CMIP6. Sci Data 9, 1–6. https://doi.org/10.1038/s41597-022-01393-4

Toimil, A., Losada, I.J., Nicholls, R.J., Dalrymple, R.A., Stive, M.J.F., 2020. Addressing the challenges of climate change risks and adaptation in coastal areas: A review. Coastal Engineering. https://doi.org/10.1016/j.coastaleng.2019.103611

Tolson, B.A., Shoemaker, C.A., 2007. Dynamically dimensioned search algorithm for computationally efficient watershed model calibration. Water Resour Res 43. https://doi.org/10.1029/2005WR004723

Tran, T.N.D., Ahmed, Z., Vo, N.D., 2021a. APPLICATION OF HYDRODYNAMIC MODELLING TO ASSESS THE EFFICIENCY OF HURRICANE PROTECTION MEASURE AT XOM RO DIKE, PHU YEN PROVINCE, VIETNAM, in: 2nd Conference on Sustainability in Civil Engineering (CSCE'20), Department of Civil Engineering Capital University of Science and Technology, Islamabad Pakistan.

Tran, T.-N.-D., Nguyen, Q.B., Zeeshan, A., 2021b. Application of Plaxis for Calculating the Construction Stability and Soft Embankment in Protecting Ha Thanh, in: 2nd Conference on Sustainability in Civil Engineering (CSCE) 2020. pp. 202–210.

Tran, T.-N.-D., Do, S.K., Nguyen, B.Q., Tran, V.N., Grodzka-Lukaszewska, M., Sinicyn, G., Lakshmi, V., 2024. Investigating the Future Flood and Drought Shifts in the Transboundary Srepok River basin Using CMIP6 Projections. IEEE J Sel Top Appl Earth Obs Remote Sens 17, 7516–7529. https://doi.org/10.1109/JSTARS.2024.3380514

Tran, T.-N.-D., Le, M.-H., Zhang, R., Nguyen, B.Q., Bolten, J.D., Lakshmi, V., 2023a. Robustness of gridded precipitation products for vietnam basins using the comprehensive assessment framework of rainfall. Atmos Res 293, 106923. https://doi.org/10.1016/j.atmosres.2023.106923

Tran, T.-N.-D., Nguyen, B.Q., Grodzka-Łukaszewska, M., Sinicyn, G., Lakshmi, V., 2023b. The role of reservoirs under the impacts of climate change on the Srepok River basin, Central Highlands of Vietnam. Front Environ Sci 11. https://doi.org/10.3389/fenvs.2023.1304845

Tran, T.N.D., Nguyen, B.Q., Vo, N.D., Le, M.H., Nguyen, Q.D., Lakshmi, V., Bolten, J.D., 2023c. Quantification of global Digital Elevation Model (DEM) – A case study of the newly released NASADEM for a river basin in Central Vietnam. J Hydrol Reg Stud 45. https://doi.org/10.1016/j.ejrh.2022.101282

Tran, T.N.D., Nguyen, B.Q., Zhang, R., Aryal, A., Grodzka-Łukaszewska, M., Sinicyn, G., Lakshmi, V., 2023d. Quantification of Gridded Precipitation Products for the Streamflow Simulation on the Mekong River Basin Using Rainfall Assessment Framework: A Case Study for the Srepok River Subbasin, Central Highland Vietnam. Remote Sens (Basel) 15. https://doi.org/10.3390/rs15041030

Tran, T.-N.-D., Nguyen, B. Q., Tran, V. N., Le, M.-H., Bolten, J., Do, S. K., Doan, V. B., Do, H. X., Arshad, A., Kantoush, S. A., Lakshmi, V., 2023e. Quantification of Climate Change impacts on the Srepok River, Mekong River basin. AGU. https://doi.org/10.22541/essoar.170365224.48937662/v1

Tran, T.N.D., Nguyen, Q.B., Nguyen, T.T., Vo, N.D., Nguyen, C.P., Gourbesville, P., 2022a. Operational Methodology for the Assessment of Typhoon Waves Characteristics. Application to Ninh Thuan Province, Vietnam, in: Springer Water. Springer Nature, pp. 887–902. https://doi.org/10.1007/978-981-19-1600-7_55

Tran, T.N.D., Nguyen, Q.B., Vo, N.D., Marshall, R., Gourbesville, P., 2022b. Assessment of Terrain Scenario Impacts on Hydrological Simulation with SWAT Model. Application to Lai Giang Catchment, Vietnam, in: Springer Water. Springer Nature, pp. 1205–1222. https://doi.org/10.1007/978-981-19-1600-7_77

Tran, T. N. D., Nguyen, B. Q., Le, M.-H., Lakshmi, V. (Venkat), Bolten, J. D., & Aryal, A., 2022c. Robustness of Gridded Precipitation Products in Hydrological Assessment for Vietnam River basins. AGU Fall Meeting Abstracts, 2022, H22M-07.

Tran, T.N.D, Nguyen, Q.B., Tam, D., Le, L., Nguyen, T.D., Vo, N.D., Gourbesville, P., 2022d. Evaluate the Influence of Groynes System on the Hydraulic Regime in the Ha Thanh River, Binh Dinh Province, Vietnam, in: Advances in Hydroinformatics. pp. 241–254. https://doi.org/10.1007/978-981-19-1600-7_15

Trang, N.T.T., Shrestha, S., Shrestha, M., Datta, A., Kawasaki, A., 2017. Evaluating the impacts of climate and land-use change on the hydrology and nutrient yield in a transboundary river basin: A case study in the 3S River Basin (Sekong, Sesan, and Srepok). Science of the Total Environment 576, 586–598. https://doi.org/10.1016/j.scitotenv.2016.10.138

Trenberth, K.E., Dai, A., Van Der Schrier, G., Jones, P.D., Barichivich, J., Briffa, K.R., Sheffield, J., 2014. Global warming and changes in drought. Nat Clim Chang 4, 17–22. https://doi.org/10.1038/nclimate2067

Ulpiani, G., 2021. On the linkage between urban heat island and urban pollution island: Three-decade literature review towards a conceptual framework. Science of the Total Environment. https://doi.org/10.1016/j.scitotenv.2020.141727

Umar, M., Khan, S.N., Arshad, A., Aslam, R.A., Khan, H.M.S., Rashid, H., Pham, Q.B., Nasir, A., Noor, R., Khedher, K.M., Anh, D.T., 2022. A modified approach to quantify aquifer vulnerability to pollution towards sustainable groundwater management in Irrigated Indus Basin. Environmental Science and Pollution Research 29, 27257–27278. https://doi.org/10.1007/s11356-021-17882-9

UN Population Division, 2018. World Urbanization Prospects: The 2018 Revision.

U.S. Census Bureau, 2020. Nation's Urban and Rural Populations Shift Following 2020 Census [WWW Document]. https://www.census.gov/programs-surveys/decennial-census/decade/2020/2020-census-results.html. No Page. No volume.

U.S. Census Bureau, 2022. Nation's Urban and Rural Populations Shift Following 2022 Census [WWW Document]. https://www.census.gov/newsroom/press-releases/2022/urban-rural-populations.html. No Page. No volume.

USGS, 2020. Land change monitoring, assessment, and projection. U.S. Geological Survey Fact Sheet 2020, 1–4. https://doi.org/10.3133/ fs20203024

Villarini, G., Smith, J.A., 2010. Flood peak distributions for the eastern United States. Water Resour Res 46. https://doi.org/10.1029/2009WR008395

Wan, X., Wang, W., Liu, J., Tong, T., 2014. Estimating the sample mean and standard deviation from the sample size, median, range and/or interquartile range. BMC Med Res Methodol 14, 135. https://doi.org/10.1186/1471-2288-14-135

Wang, T., Tu, X., Singh, V.P., Chen, X., Lin, K., 2021. Global data assessment and analysis of drought characteristics based on CMIP6. J Hydrol (Amst) 596, 126091. https://doi.org/10.1016/j.jhydrol.2021.126091

Wood, A.W., Leung, L.R., Sridhar, V., Lettenmaier, D.P., 2004. Hydrologic implications of dynamical and statistical approaches to downscaling climate model outputs. Clim Change 62, 189–216. https://doi.org/10.1023/B:CLIM.0000013685.99609.9e

Wood, A.W., Maurer, E.P., Kumar, A., Lettenmaier, D.P., 2002. Long-range experimental hydrologic forecasting for the eastern United States. Journal of Geophysical Research: Atmospheres 107, ACL 6-1-ACL 6-15. https://doi.org/10.1029/2001JD000659

Xu, X., Yun, X., Tang, Q., Cui, H., Wang, J., Zhang, L., Chen, D., 2023. Projected seasonal changes in future rainfall erosivity over the Lancang-Mekong River basin under the CMIP6 scenarios. J Hydrol (Amst) 620, 129444. https://doi.org/10.1016/j.jhydrol.2023.129444

Yin, D., Harris, C., Tran, T. N. D., Tapas, M., Etheridge, J. R., Moysey, S. M., & Lakshmi, V. V. (2024, February). Effects of Sea-Level Rise and River Flow Variation on Estuarine Salinity in a Changing Climate: Insights from the Pamlico River Estuary, USA. In 2024 Ocean Sciences Meeting. AGU.

Yin, Y., Wu, Y., Bartell, S.M., Cosgriff, R., 2009. Patterns of forest succession and impacts of flood in the Upper Mississippi River floodplain ecosystem. Ecological Complexity 6, 463–472. https://doi.org/10.1016/j.ecocom.2009.08.004

Yun, X., Tang, Q., Li, J., Lu, H., Zhang, L., Chen, D., 2021. Can reservoir regulation mitigate future climate change induced hydrological extremes in the Lancang-Mekong River Basin? Science of the Total Environment 785, 147322. https://doi.org/10.1016/j.scitotenv.2021.147322

Zhang, T., Yang, J., Winrich, A., Will, R.E., Zou, C.B., 2024. Trade-off of ecosystem productivity and water use related to afforestation in southcentral USA under climate change. Science of The Total Environment 915, 170255. https://doi.org/10.1016/j.scitotenv.2024.170255

Zhang, W., Zheng, C., Chen, F., 2019. Mapping heat-related health risks of elderly citizens in mountainous area: A case study of Chongqing, China. Science of the Total Environment 663, 852–866. https://doi.org/10.1016/j.scitotenv.2019.01.240

Zhang, Y., Liu, H., Qi, J., Feng, P., Zhang, X., Liu, D.L., Marek, G.W., Srinivasan, R., Chen, Y., 2023. Assessing impacts of global climate change on water and food security in the black soil region of

Northeast China using an improved SWAT-CO2 model. Science of the Total Environment 857. https://doi.org/10.1016/j.scitotenv.2022.159482

Zhong, R., Zhao, T., Chen, X., Jin, H., 2022. Monitoring drought in ungauged areas using satellite altimetry: The Standardized River Stage Index. J Hydrol (Amst) 612, 128308. https://doi.org/10.1016/j.jhydrol.2022.128308

Zhou, Z., Ding, Y., Fu, Q., Wang, C., Wang, Y., Cai, H., Liu, S., Huang, S., Shi, H., 2023. Insights from CMIP6 SSP scenarios for future characteristics of propagation from meteorological drought to hydrological drought in the Pearl River Basin. Science of the Total Environment 899. https://doi.org/10.1016/j.scitotenv.2023.165618